Energy Conversion and Management: X 24 (2024) 100796

Contents lists available at ScienceDirect

Energy Conversion and Management: X

journal homepage: www.sciencedirect.com/journal/energy-conversion-and-management-x

Parametric optimization of engine performance and emissions for hydroxy blended gaseous fuels

Muhammad Ali Ijaz Malik [a,*], Adeel Ikram [b,c,*], Shayan Sohail [c], Muhammad Naqvi [d], Muhammad Khubaib [e], Fayaz Hussain [f,*], Bo Zhang [g,*]

[a] School of Civil and Environmental Engineering, FEIT, University of Technology Sydney, NSW 2007, Australia
[b] Faculty of Engineering, Chungnam National University, Daejeon, Republic of Korea
[c] Department of Mechanical Engineering, Superior University, Lahore, Pakistan
[d] College of Engineering and Technology, American University of the Middle East, Kuwait
[e] Department of Mechanical Engineering, University of Engineering and Technology, Lahore, Pakistan
[f] Department of Biological and Agricultural Engineering, Faculty of Engineering, Universiti Putra Malaysia, Selangor, Malaysia
[g] School of Mechanical Engineering, Ningxia University, China

ARTICLE INFO

Keywords:
Engine performance
Environmental emissions
Hydroxy gas
Sustainable future
Renewable fuels

ABSTRACT

Gaseous fuels, such as liquefied petroleum gas (LPG) and compressed natural gas (CNG), present a promising alternative to gasoline but with a major drawback due to their lower power output. This study focuses on enhancing power production by combining gaseous fuels with hydroxy gas (HHO), generated via water electrolysis, due to its renewable nature and favorable physiochemical properties. The current study uniquely improves CNG and LPG engine performance by supplementing with HHO gas, compensating for lower efficiency and power than gasoline. Additionally, it innovatively applies response surface methodology (RSM) with a central composite design (CCD) to optimize and analyze fuel blend effects on engine performance. Operating an engine at 1600 to 3400 rpm with a 60 % open throttle, it was observed that, on average, LPG and CNG yielded 23.67 % and 18.91 % lower torque than gasoline. However, adding HHO gas increased torque by 6.57 % for LPG and 6.32 % for CNG. Moreover, LPG-HHO and CNG-HHO blends exhibited 22.66 % and 24.01 % higher brake thermal efficiency (BTE) and 30.44 % and 35.70 % lower brake specific fuel consumption (BSFC) compared to gasoline, respectively. Adding HHO in LPG and CNG reduced CO_2 emissions by 7.69 % and 8.2 %, respectively, while increasing NOx emissions by 12.92 % and 12.10 %, respectively. However, this reduction in hazardous pollutant release plays a significant role in ecosystem sustainability. Using RSM, an overall desirability of 0.731 was achieved, pinpointing optimized conditions for a CNG-HHO fuel blend at an engine speed of 2757 rpm. Under such conditions, the observed values were: brake torque of 7.94 Nm, brake power (BP) of 2.14 kW, BSFC of 0.35 kg/kWh, BTE of 23.5 %, CO of 796.24 ppm, CO_2 of 6.84 %v, HC of 97.07 ppm, and NOx of 281.6 ppm. Experimental outcomes aligned with the trends predicted by RSM and CCD. Both methodologies highlight the most favorable conditions for the CNG-HHO blend. Applying RSM saves time and minimizes expenses that would otherwise be incurred in extensive experimentation.

Introduction

Over the last few decades, industrialization and population explosion have resulted in an immense increase in fossil fuel consumption, ultimately reflected in their depletion[1]. As per projections, the global population is escalating at a frequency of 83.1 million annually. [2]. Energy Information Administration has quantified that energy consumption worldwide is anticipated to rise by 56 % in 2040 compared to 2010 [3]. It is projected that fossil fuels may be exhausted within the next 50 years if consumption continues at the current rate [4]. Adopting suitable alternative fuels for the existing vehicles could prolong the lifespan of fossil fuel reserves and reduce environmental pollution for a further 10 to 20 years [5,6]. Hydrocarbon fuels are the primary

* Corresponding authors.
E-mail addresses: muhammadaliijaz.malik@student.uts.edu.au (M.A. Ijaz Malik), dr.adeelikram@gmail.com, adeel.ikram@superior.edu.pk (A. Ikram), shayan.sohail507@gmail.com (S. Sohail), sayed.naqvi@aum.edu.kw (M. Naqvi), mkhubaib111@gmail.com (M. Khubaib), fayazhussain@upm.edu.my (F. Hussain), zhangb@nxu.edu.cn (B. Zhang).

https://doi.org/10.1016/j.ecmx.2024.100796
Received 19 September 2024; Received in revised form 11 November 2024; Accepted 13 November 2024
Available online 16 November 2024

Nomenclature

ANOVA	Analysis of variance
BP	Brake power
BSFC	Brake-specific fuel consumption
BTE	Brake thermal efficiency
CCD	Central composite design
CNG	Compressed natural gas
CO	Carbon monoxide
CO_2	Carbon dioxide
CV%	Coefficient of variance
CCDOE	Central composite design of experiment
EGT	Exhaust gas temperature
G	Gasoline
HP	Horsepower
HC	Hydrocarbon
HHO	Hydroxy gas
LPM	Litres per minute
LPH	Litres per hour
NO_X	Oxides of nitrogen
RSM	Response surface methodology
R^2	Regression coefficient
scfh	Standard cubic feet per hour
SI	Spark ignition
Std.Dev.	Standard deviation
WOT	Wide open throttle

contributor to carbon emissions and ecosystem deterioration [7]. Therefore, the rapid exhaustion of fossil fuel sources, fluctuating fuel prices, and alarming environmental hazards have pushed scientists to seek sustainable fuel resources [8–10]. A major source to meet the population's demand for energy is petroleum fuels. In 2015, the overall primary energy consumption worldwide included 4.7 % nuclear power, 85.6 % fossil fuel, and 9.7 % renewable energy [2]. The large share of fossil fuel in the energy mix depicts the production of harmful exhaust gases to the environment, resulting in global warming and environmental degradation.

The global energy requirement of the transportation sector is predicted to increase by 70 % from 2010 to 2040; 60 % of this increase will impact only heavy-duty vehicles [11]. As a substantial consumer of conventional fuels, the automotive sector is mainly responsible for the exhaust emissions that harm the environment. The resultant exhaust emissions are nitrogen oxides, carbon monoxide, and various unburned hydrocarbons [12,13]. The transportation industry consumes 18 % of world energy and accounts for 23 % of the world's CO_2 emissions, resulting in global warming [14]. Despite the eco-friendly nature of renewable fuels, social, economic, and technical constraints exist in their adoption as primary fuel. However, much research has already been done on alternative fuels (alcohols, CNG and, LPG) in SI engines due to lower environmental emissions [15–17]. However, the major drawback of employing alternative fuel is lower power production than gasoline for the same engine operating condition due to lower calorific value [18,19]. LPG-powered motors are potentially profitable due to their higher-octane qualities, faster flame propagation capacity, and improved auto-ignition temperatures. It is a fine quality, less harmful combination of hydrocarbons found in nature, primarily propane and butane. As a result, a reduced carbon-hydrogen composite reduces the potential harm to the vehicle engine and engine exhaust [20–22].

Natural gas, usually compressed at probably lower temperatures (−161 °C), possesses a higher octane rating and lower density than gasoline. The existing literature prescribes that CNG is capable of running under higher compression ratios and turned out to be a safer fuel because of higher ignition temperature and lesser chances of leakage [23]. Moreover, CNG prompted higher advantages in terms of engine emissions than gasoline. The CO_2 formation depends on fuel composition with several carbon atoms. As CNG is principally considered as methane, due to a single carbon atom per molecule, CO_2 emissions are significantly reduced. The combustion of CNG takes place under stoichiometric air-fuel ratio conditions, resulting in a substantial decrease in CO emissions. Moreover, the minimal crevice leakage, higher combustion temperature, and lean combustion in the case of CNG are responsible for lower HC emissions and higher NO_x [24]. The advanced spark timing to compensate for the lower flame speed of CNG and no cooling, which resulted from liquid fuel vaporization, mainly results in higher temperature, which ultimately leads to higher NO_x emissions [25]. Mohammed et al. [26] found higher NO_x emissions in the case of CNG and obtained irregular NOx trends through the engine thermal management system.

To cope with gaseous fuels' storage and safety issues, it turned out to be a sensible approach to use an HHO generation unit to produce hydroxy gas [27]. The literature review reveals that lower thermal efficiencies and poor burning are obtained through conventional fuels. However, an improvement can be made by blending LPG and CNG with hydrogen [28–31]. Hydrogen's robustness and the complexity involved in its storage limit its application in automotive [32–34]. As a result, researchers are concentrating on hydroxy gas, which can be created by utilizing an onboard hydrogen generating system. It should be noted that hydroxy gas is a 2:1 M (or volume) blend of oxygen and hydrogen gas. The HHO gas comprises 89 % molecular oxygen and 11 % molecular hydrogen [34–36]. The oxygen content in hydroxy gas is responsible for improved combustion inside engine cylinders that may reflect in higher brake power, higher thermal efficiency, and lower fuel consumption at the cost of higher NOx emissions [37,38]. Hydrogen became a favorable fuel because of its higher flame and dispersion rates, large ignitability range, and lower viscosity [27,39]. The hydrogen content in hydroxy gas mainly decreases CO and HC emissions, ultimately resulting in higher thermal efficiency [40]. Since HHO is made solely from water electrolysis, a renewable resource, it is a sustainable fuel due to its inherent existence. Since HHO has minimal carbon content, hydroxy gas burns more effectively than coal and other fuels [41,42]. HHO can be created by electrolyzing water molecules atoms (apparently 67 % vol. H_2 and 33 % vol. O_2) [43]. Also, its calorific value is exceptionally high compared to gasoline and diesel. One kilogram of HHO has a calorific value of 3.2 and 3 times larger than diesel and petrol [44,45].

Simsek and Uslu [46] conducted experiments on LPG and gasoline under full and half-throttle conditions. They found that LPG produced a 34.19 % increase in the BSFC under full-throttle opening and a reduction (8.95 %) in BTE compared to gasoline. Moreover, they observed a decrease of 62.03 % in CO emissions, a 63 % decline in HC emissions, and a 56.42 % decline in CO_2 emissions for LPG in contrast with gasoline. For half-throttle opening (HTO), BSFC was incremented by 45.51 %, while BTE declined by 20.22 % for LPG. In addition, a decrease of 47.65 % in CO, 62.38 % in HC, and 69.54 % in CO_2 emissions was observed for LPG. Also, cylinder pressures decreased by about 24.41 % for LPG. Ahmet and Yahya [47] found lower HC and CO emissions and BSFC for CNG fuel at partial loading conditions and varying engine speeds. Besides the significant decline in CO_2, HC, and CO contents, Khanh et al. [48] reported lower NOx emissions for CNG than gasoline. Hydroxy gas consists of hydrogen (H_2) and oxygen (O_2) by a volume 2:1 (HHO), and its blend with CNG and LPG fuel is responsible for optimized engine performance along with a significant decline in exhaust emissions [49,50]. Wang et al. [51] ascertained the effect of a 3 % HHO addition on SI engine performance and found considerable improvement in BTE, CO, and HC emissions. Lee et al. [52] stated improved fuel consumption and efficiency for all lambda values and spark timing

conditions for HCNG upon comparison with CNG. Hydrogen addition to CNG (HCNG) results in approximately 25 % reduction in energy consumption, ultimately leading to higher combustion efficiency. Mathai et al. [53] stated a 59.1 % increase in NOx emissions for hydrogen-enriched CNG under constant loading and speed conditions.

Appendix compares the results of the current study with those of previous research. Almost all researchers agree that adding LPG, CNG, and HHO decreases exhaust emissions. However, Cakmak et al. [54] presented an increase of 2.22 – 6.42 % in NOx emissions with the addition of hydroxy gas in LPG. Likewise, most researchers portray that the engine power decreases, torque decreases, BSFC decreases, and BTE increases for LPG, CNG, and HHO. However, some exceptional cases are reported by Çakmak et al. [54] in terms of brake power, Yilmaz [41] and Falahat et al. [55] in terms of torque, Simsek and Uslu [46] in terms of BSFC and Hashem et al [56] in terms of BTE.

The predictive models offer the unique benefit of analyzing the interaction between process variables on the desired output [57]. It helps identify the simultaneous impact of multiple factors on desired output. Response surface methodology (RSM) analyzes the synergetic interactions between input/output parameters by displaying 3D surface plots [58]. RSM can handle linear and non-linear associations using first-order (linear) or second-order (quadratic) polynomial models. Because of its adaptability, RSM may be applied to various systems, ranging from simple systems with a small number of variables to intricate ones with numerous interrelated elements [59]. Central Composite Design (CCD) in RSM is a statistical, empirical design approach used to assess the optimal operating conditions for an experiment [60]. RSM allows multi-objective optimization with multiple targets and input parameters [61]. In many optimization approaches, achieving one target results in a compromise over other parameters. Therefore, multi-objective optimization portrays a trade-off between targets and input that may result in improved decision-making [62]. ANOVA helps verify whether the RSM model accurately represents the data by examining the statistical significance of the entire model [63]. A significant model indicates that the relationship between input variables and response is meaningful and not due to random variation, increasing confidence in the optimization results [64]. ANOVA assists in confirming whether the RSM model appropriately depicts the data when analyzing the statistical significance of the RSM proposed model [65]. Confidence in the optimization outcomes is increased when a substantial model shows that the relationship between input variables and response is meaningful and not the result of random variation [66]. Ghanbari et al. [67] used RSM to statistically analyze the experimental results and predict the results for engine and emissions parameters. The R-squared values ascertained for brake power, BSFC, brake torque, NOx, CO_2, CO, and HC were 0.99, 0.98, 0.99, 0.88, 0.92, 0.96, and 0.96, respectively. Taghinezhad et al. [68] optimized the performance of a dual-rotor ducted wind turbine through RSM, and predicted models with a p-value less than 0.05, highlighting its significance. Paneerselvam et al. [69] employed RSM to optimize the ultrasound-assisted melia dubia oil extraction with green solvents. Using 2-methyl tetrahydrofuran and an extraction time of 87.6 min, ANOVA analysis has determined the ideal solvent-to-solid ratio, solvent type, and extraction time to be precisely 6.98 mL/g. With these conditions, the maximum yield of 50.3 % for Melia dubia oil was obtained. With an error margin of just 0.28 percent, the ANOVA analysis enabled extremely precise forecasts of oil yield.

The current study portrays a novel approach for improvement in engine performance in the case of CNG and LPG by supplementing the fuel system with HHO. HHO is known for its ability to enhance combustion and was introduced to balance the lower performance characteristics of CNG and LPG compared to gasoline. This innovative fuel combination, intended to balance efficiency and emissions, addresses key limitations of alternative fuels in SI engines. Furthermore, applying RSM with a CCD to analyze and optimize the empirical data adds an additional layer of novelty. By applying this advanced statistical approach, the study comprehensively evaluates the interaction effects between LPG, CNG and HHO on engine performance. This combination of empirical approach and RSM analysis offers valuable insights into optimizing alternative fuel usage in SI engines, paving the way for future research on fuel efficiency and emissions reduction strategies. The current study addresses the following research questions:

- How does the engine behave for hydroxy blended LPG and CNG fuel?
- How much power can be compensated through hydroxy gas?
- To what extent can exhaust emissions be reduced through hydroxy blended gaseous fuels?
- How can the CCD of an experiment work for an SI engine?
- To what extent can optimized results be achieved?

Methodology

Experimental setup

A schematic layout of all the testing equipment and auxiliaries connected to the test engine is presented in Fig. 1. The Kart dynamometer of Dynomite company, with a 7-inch diameter, is attached to the engine through a shaft to measure the engine speed and torque. Air first enters the system through a hygrometer, which measures the humidity level in the air, which is then filtered through an air filter. HHO is entered after passing through wet and dry flame arrestors to ensure safety and avoid backfire. The air is then mixed with test fuels, either CNG, LPG, HHO, or gasoline, and supplied to the engine through a carburetor. A SI engine was used in the experiment; the specifications are given in Table 1. The probe of the emissions analyzer was inducted into the exhaust duct of the engine to ascertain NOx, CO, CO_2 and HC emissions. The Data Acquisition System is a laptop on which Dyno-Max 2010 software has been installed, and the software interface displays all the ascertained parameters.

Test fuels

A graded measuring cylindrical tube of 1 % resolution on full-scale reading (measurement range 0 to 1000 mL) was used to deliver gasoline and measure its gasoline consumption, whereas a CNG cylinder was positioned on a weighing machine (resolution = 0.1 g), which weighed the comparative change in weight upon the consumption of gas. At 1.1 bar pressure, CNG and LPG were supplied to the intake engine duct. Two valves were located on the crossover kit; one was for safety purposes, and the second was to regulate the gas pressure around 1.1 bar, comparatively higher than the intake pressure. The CNG and LPG at 1.1 bar and HHO at 10 scfh/4.72 LPM are subsequently inducted into the engine for HHO-CNG and HHO-LPG blend combustion. The lower flow rates are selected to ensure safer engine operation without compromising engine integrity or causing undesirable combustion phenomena like pre-ignition or knocking. Previous researchers have also selected such lower flow rates of HHO to prevent any potential safety hazards associated with higher HHO concentrations [37,38]. HHO unit consists of an anode and cathode, dipped into electrolyte for hydroxy gas generation through the electrolytic reaction mentioned below [29]. HHO was produced from an electrolytic cell of dimension 16.5 x 16.5 x 0.1 cm^3, input voltage of about 35 V, and input current of about 0–60 A, having 24 stainless-steel plates (316 L) with 2 mm distance among them. The reactor consists of two cathodes at the boundary and 2 anode plates positioned at the center, separated with a seal. Distilled water and 6 g/liters of potassium hydroxide (KOH) were catalysts [70]. KOH is used as the ion conductivity element in the generation of HHO, similar to its application in previous studies [71]. However, the HHO is generated through the water electrolysis in an electrolytic cell. At the cathode, water disintegrated into hydrogen (H_2) and hydroxide (OH–) ions (see Equation (1)). At the anode, hydroxide ions disintegrated to yield water molecules and oxygen, as mentioned in Equation (2). The water molecules tend to produce HHO, as seen in Equation (3):

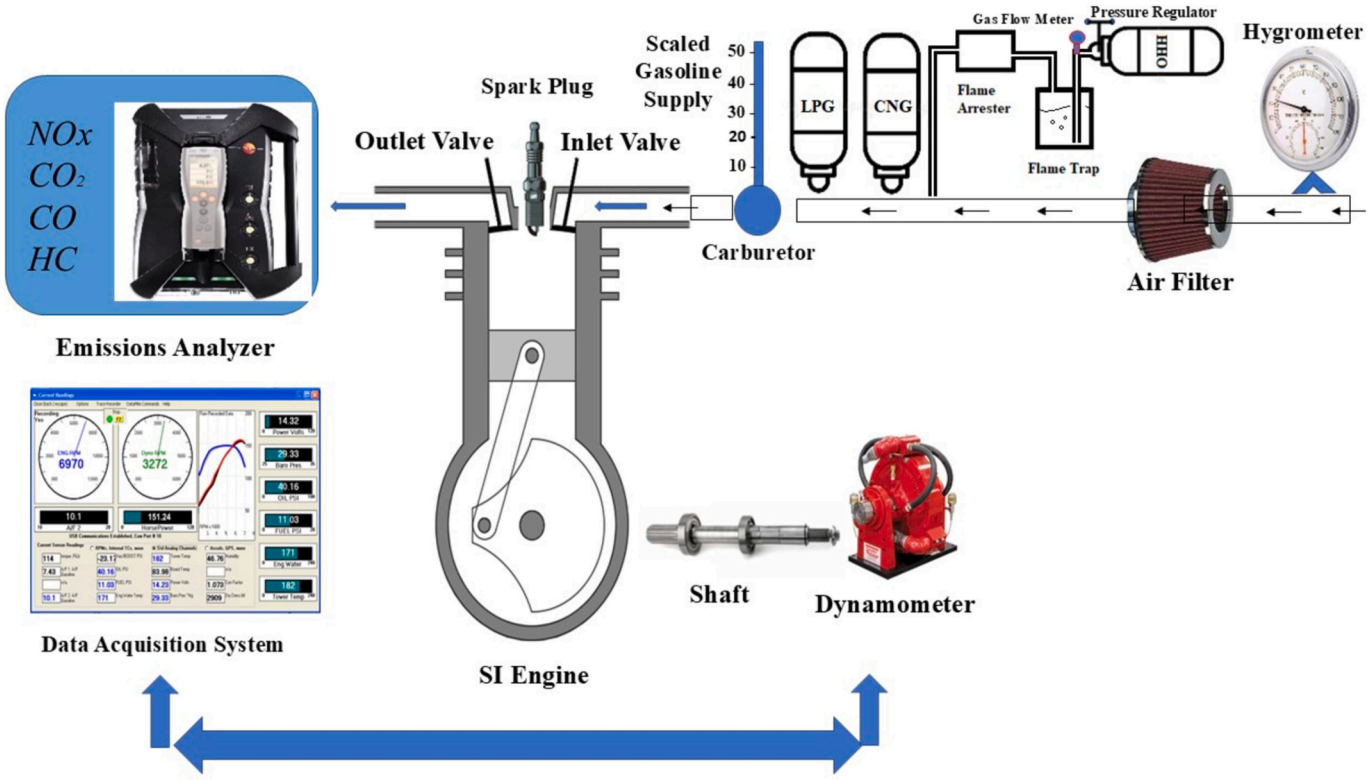

Fig. 1. Schematic of the experimental setup.

Table 1
Test engine specifications.

Characteristics	Specification
No. of strokes	4
Bore	67 mm
No. of cylinder	1
Stroke	62.2 mm
Compression ratio	9.5:1
Nature of cooling	Water cooled
Maximum power	7.4 kW
Ignition type	Spark
Displacement	219 cc

$$Cathode\,Site: 4H_2O + 4e^- \rightarrow 2H_2 + 4OH^- \quad (1)$$

$$AnodeSite: 4OH^- \rightarrow O_2 + 2H_2O + 4e^- \quad (2)$$

$$Completereaction: 2H_2O \rightarrow 2H_2 + O_2 \quad (3)$$

Adequate ventilation in the laboratory prevents the accumulation of HHO gas at a single point. A laboratory safety alarm is used for timely caution in case of HHO leakage. To prevent HHO backflow and avoid dangerous conditions, a check valve with a back-pressure capacity (> 0.3 MPa) is used. The rubber gloves and fire extinguishers are used as necessary precautions. Both wet and dry-type flame arrestors are positioned for safety precautions to avoid backfire. In dry flame arrestors, a series of perforated plates (metal mesh) are used to quench flames as they initiate turbulence, which disperses the flame's energy and dampens it down. In wet flame arrestors, the cooling fluid suppresses flame through saturation. The properties of fuels are mentioned in Table 2.

Test scheme

SAE J1349 standard was followed to ascertain the torque through the dynamometer. The water brake dynamometer comprised of toroidal pockets driven by the engine and was used in the experiment. A 1 HP motor was used to supply water to the dynamometer, acting as an engine load. The load control valve regulated the water supply to change the load. The basic phenomenon inside the dynamometer is that water is whipped around toroidal pockets, and the shear forces produced in the water are directed peripheral to the housing radius of the dynamometer. The shear forces act as a load on the engine. The engine speed was minimal when the load on the engine was maximum, and the engine speed started increasing when the load on the engine was regulated to decrease through the load control valve. Testo-350 emissions analyzer was used to measure exhaust emissions. It measured NO_x within the range of 0 to 4000 ppm with an accuracy of ± 1 ppm, CO_2 within the range of 0 to 50 % with an accuracy of ± 0.3 %, CO within the range of 0 to 10,000 ppm with an accuracy of ± 5 ppm, HC emission within range of 100 to 18000 ppm with an accuracy of ± 2 %. Firstly, the experiment was performed on subsequent fuels before it was performed on HHO blended to compare with base fuels (LPG, CNG, and gasoline). Table 3 displays the detailed experimental approach.

Table 2
Test fuel properties.

Properties	ASTM standards	CNG Gas-Phase	LPG Gas-Phase	Gasoline Liquid-Phase	HHO Gas Phase
Density (kg/liter at 15.48 °C)	D1298	0.128	0.00189	0.74	0.0827[a]
Research octane number	D2699	120	103	92	> 130
Air-to-fuel ratio	–	17	17.2	14.75	34.2
Flame speed (m/s)	D7538	0.41	1.5	0.5	2.65
Calorific value (MJ/kg)	D240	49	46.1	46	120

[a] Density in kg/m^3 at 0 °C and 1.01 × 10^5 Pa.

Table 3
Comprehensive test strategy.

Factors	Description
Throttle condition	60 % wide open throttle (WOT)
Fuel type	LPG, CNG, LPG-HHO, CNG-HHO and gasoline
Speed range	1600 to 3300 rpm with 400 rpm interval
Load applied	15 to 50 psi
Performance characteristics	Torque, BP, BSFC and BTE
Emission characteristics	NO_x, CO, CO_2 and HC
Ambient temperature	25 °C
Ambient pressure	101325 Pa

Uncertainty analysis

Table 4 displays the uncertainty associated with the instruments used in the experimentation, their accuracy, and measurement range. Uncertainty analysis is significant for assessing the credibility of empirical findings. The statistical significance of ascertained results can be determined through uncertainty linked with measured parameters.

The overall experimental uncertainty is evaluated by known errors linked with the parameters through the help of the general equation (4) [72] as follows:

$$\frac{\varnothing_y}{y} = \sqrt{\sum_{i=1}^{n}\left(\frac{1}{y}\frac{\partial y}{\partial x}\varnothing_{x_i}\right)^2} \tag{4}$$

where $\varnothing_{x_i}$ and $\varnothing_y$ and are the uncertainties and errors in x_i and y, respectively, and x_i are the determined physical parameters. Equation (4) is used to calculate the experiment's uncertainty. Inserting error percentages from Table in equation (4) leads to:

$$\varnothing_{exp} = \left[\left(\left(\varnothing_{power}\right)^2 + \left(\varnothing_{speed}\right)^2 + \left(\varnothing_{torque}\right)^2 + \left(\varnothing_{BTE}\right)^2 + \left(\varnothing_{BSFC}\right)^2 + \left(\varnothing_{HC}\right)^2 + \left(\varnothing_{NOx}\right)^2 + \left(\varnothing_{CO}\right)^2 + \left(\varnothing_{CO_2}\right)^2\right)^{\frac{1}{2}}\right]$$

$$\varnothing_{exp} = \left[\left((0.5)^2 + (1)^2 + (0.2)^2 + (0.5)^2 + (0.4)^2 + (0.2)^2 + (0.2)^2 + (0.2)^2 + (0.2)^2\right)^{\frac{1}{2}}\right]$$

$$\varnothing_{exp} = 1.34\%$$

Response surface methodology

RSM is a mathematical and statistical technique utilized to model and optimize experimental outcomes in collaboration with numerical experiments. The DOE predicted by RSM is of primal importance and could be effectively used for prediction beyond the range of the designated parameter, thus saving enormous time and capital. The gasoline is designated as fuel 1, LPG is designated as fuel 2, LPG-HHO is designated as fuel 3, CNG is designated as fuel 4, and CHG-HHO is designated as fuel 5. RSM is multi-objective optimization with multiple targets. In the current study, the targets for achieving maximum power, maximum fuel efficiency, lower fuel consumption and lower emissions have been set. Table 5 includes the CCD proposed input parameter combinations as the optimum conditions for the best possible output per the set target.

RSM model employs a quadratic polynomial model to assess how input parameters affect response variables. A CCD was employed to determine the relationship between input parameters and a set of variable responses. Fuel blend and engine speed were used as two independent variables to predict models of torque, brake power, BSFC, BTE, CO, CO_2, HC and NOx at three levels (−1,0,1). For assessing the pure error, CCD consists of 13 experimental runs with four axial points, four factorial points, and five duplicated center points. Table 6 specifies the data points to identify, duplicate, factorial, and axial points.

Table 4
Measurement range, Accuracy and Uncertainty associated with parameters.

Parameter	Measurement range	Accuracy	Uncertainty
Speed	0 –7500 rpm	±5 rpm	±0.5
Torque	0 –45 Nm	±0.1 Nm	±1
Power	0 –45 kW	±0.45 kW	±0.2
BTE	–	–	±0.5
BSFC	–	±0.1 g/kWh	±0.4
NO_X	0 –5000 ppm	±1 ppm	±0.2
HC	0 –5000 ppm	±1 ppm	±0.2
CO_2	0 – 17 vol%	±0.01 vol%	±0.2
CO	0 – 17 vol%	±0.01 vol%	±0.2

Results and discussion

The experiment encompasses the analysis of five separate test fuels, i.e., gasoline, LPG, LPG-HHO, CNG-HHO, and CNG, to determine performance metrics such as torque, BSFC, and brake power. Additionally, the emission characteristics of these fuels were observed and analyzed concurrently.

Engine performance based on experimental approach

Fig. 2 illustrates that gaseous fuels generate lower torque than liquid fuels. On average, LPG and CNG produced torque values 22.60 % and 18.19 % lower than gasoline (G). This decrease can be attributed to factors such as unchanged ignition timing and methane (CH_4) characteristics, which constitute a major portion of these fuels, possessing the lowest flame velocity among hydrocarbons. Consequently, sustained combustion reduces torque as unburned hydrocarbons escape through exhaust gases due to undesired heat transfer [73]. CNG displayed approximately 4.41 % higher torque than LPG. However, introducing HHO equalized the torque between liquid and gaseous fuels. On average, LPG-HHO and CNG-HHO exhibited torque values 16.77 % and 11.25 % lower than gasoline. This signifies a 5.83 % and 6.94 % torque improvement after adding HHO to LPG and CNG. This enhancement is attributed to combining HHO with CNG and LPG, resulting in increased flame velocity, broader lean-burning limits, and reduced quenching distance. Moreover, it amplifies the lean-burning capabilities of gaseous-fueled engines when blended with hydrogen. Another contributing factor is the higher heating value of H_2 fuels, generating more torque compared to CNG and LPG alone [74,75]. Introducing HHO into the air-fuel mixture also enhances the octane rating of gasoline, potentially improving engine operability under higher compression ratios and ultimately enhancing efficiency. However, adjusting the ignition advance timing is essential to maximize engine torque without inducing engine

Table 5
CCD proposed Input parameter combination.

Fuel type	3	5	1	1	3	3	5	3	3	5	3	1	3
Engine speed	2450	3300	3300	1600	2450	2450	2450	3300	1600	1600	2450	2450	2450

Table 6
Central composite design (CCD) elements.

CCD elements	
Centre duplicate points	(x_1,x_2) => (0,0)
Factorial points	(x_1,x_2) => (1,1), (1,-1), (−1,-1), (−1,1)
Axial points	(x_1,x_2) => (1,0), (0,1), (−1,0), (0,-1)

knocking [70]. Falahat et al. [55] reported a 1 to 12.6 % increase in torque for adding HHO in gasoline from 1 to 2 LPM. However, Yontar and Dogu [76] reported a decrease in torque up to 12.7 % for CNG compared to gasoline. Ristovski et al. reported a decrease in torque of 13 % for LPG compared to gasoline and justified this decline with the decrease in volumetric efficiency in the case of LPG [77].

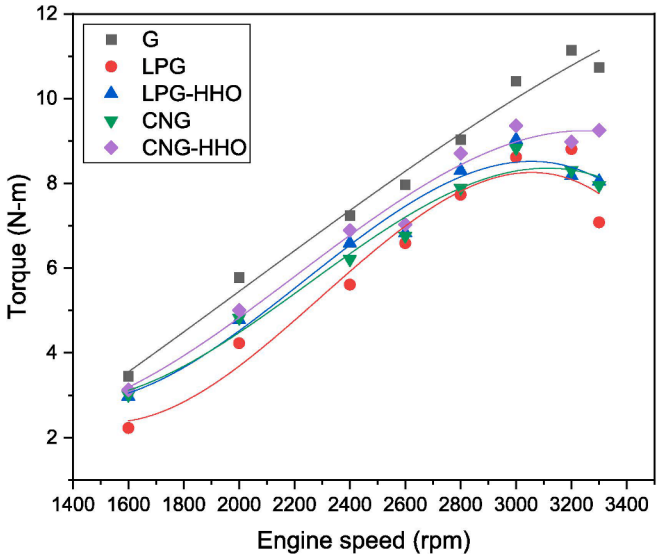

Fig. 2. Torque comparisons at various engine speeds for gasoline, CNG, CNG-HHO, LPG, and LPG-HHO blend.

The power available at the crankshaft after accounting for the losses is termed brake power. Fig. 3 depicts that gaseous fuel produced lower BP than liquid fuel. On average, LPG and CNG produced 23.67 and 18.91 % lower BP than gasoline (G). The CNG produced approximately 4.76 % higher torque than LPG. However, HHO compensated the BP between liquid and gaseous fuel. On average, LPG-HHO and CNG-HHO produced 17.10 and 12.59 % lower BP than gasoline. It means the BP regained by 6.57 and 6.32 % after supplementing HHO gas with LPG and CNG, respectively. Two major factors that can contribute to the loss of BP include lower flame velocity and air displacement. Gasoline continues to use the same quantity of suction air, but gaseous fuels, such as HHO-LPG and HHO-CNG, replace the air, leading to lower energy density than liquid fuel. For gaseous fuels, there should be a noticeable reduction in BP. But when HHO is combined with LPG and CNG, the BP rises since HHO has a larger heating value than CNG and LPG alone [73]. Çakmak et al. [54] reported an increase in BP from 1.24 to 5.04 % as the flowrate of HHO increased in LPG from 1 to 4 LPM. Jahirul et al [78] reported a decrease in BP of 19.25 % for CNG compared with gasoline. Gad et al. blended HHO gas with gasoline and observed an increase in BP of 16.52 % [79].

BSFC serves as a degree of fuel efficiency of a prime mover that ignites the fuel and generates rotational or shaft power. BSFC for test fuels across the defined range of engine speed is shown in Fig. 4. All fuels showed a similar trend in which the value of BSFC decreased at first, then increased with increasing speed. On average, LPG and CNG produced 14.67 and 25.67 % lower BSFC than gasoline (G). This drop can be attributed to the higher energy potential and passive burning of CNG and LPG. Furthermore, increased frictional power at higher engine speeds may reduce the growth rate in brake power while improving fuel consumption. CNG produced approximately 11 % lower BSFC than LPG. This is because CNG has a higher heating value than LPG. As the heating value decreases, the BSFC value increases [73]. BSFC was further reduced with the introduction of HHO as a blend with LPG and CNG due to improvement in combustion efficiency, and the HHO supplied a more

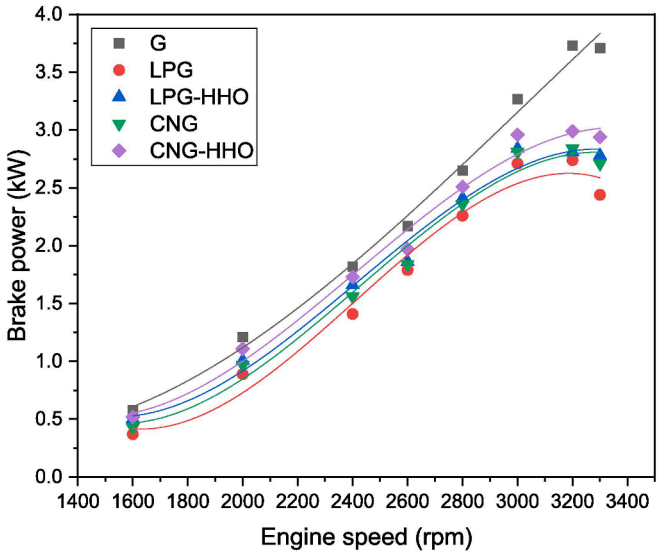

Fig. 3. Comparisons of BP at various engine speeds for gasoline, CNG, CNG-HHO, LPG, and LPG-HHO blend.

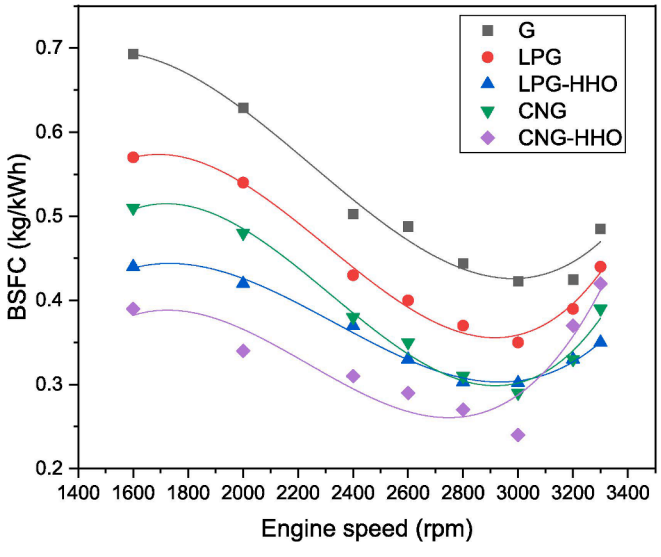

Fig. 4. Comparisons of BSFC at various engine speeds for gasoline, CNG, CNG-HHO, LPG, and LPG-HHO blend.

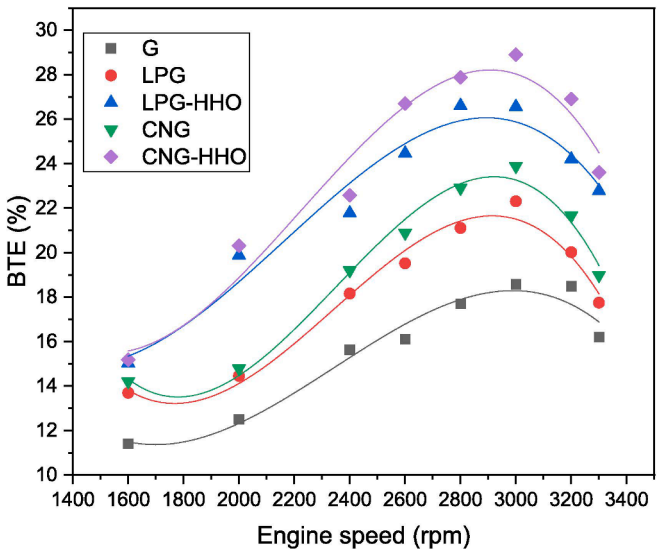

Fig. 5. Comparisons of BTE at various engine speeds for gasoline, CNG, CNG-HHO, LPG, and LPG-HHO blend.

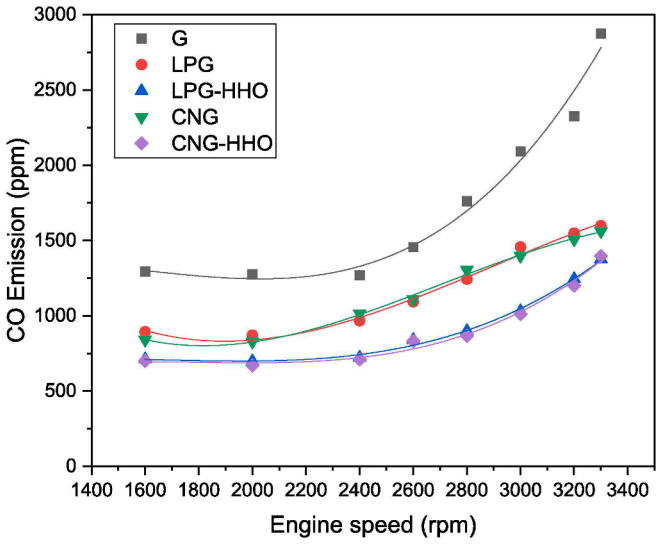

Fig. 6. Comparisons of CO emission at various engine speeds for gasoline, CNG, CNG-HHO, LPG, and LPG-HHO blend.

homogenous mixture with air due to its higher diffusivity [80]. On average, LPG-HHO and CNG-HHO produced 30.44 and 35.70 % lower BSFC than gasoline. This trend can be reasoned to the higher calorific value of the LPG-HHO and CNG-HHO blend in contrast to the gasoline alone. The higher the BSFC is because of the lower calorific value since a lower calorific value of fuel requires a larger fuel consumption to generate the same amount of power [27,81]. EL-Kassaby et al. [70] reported a 34 % decrease in BSFC for gasoline and HHO blended fuel. Çakmak et al. [54] reported a 2.92 to 11.17 % decrease in BSFC for LPG, gasoline, and HHO mixture. Yontar and Dogu [76] reported a 16.5 % decrease in BSFC for CNG compared with gasoline.

BTE is the ratio of the fuel energy the engine provides to the brake power acquired from the engine. BTE determines the extent of heat, which is transformed into work. BTE primarily relies on factors such as engine design, applications, and fuel type. It can be observed from Fig. 5 that the gaseous fuel burns more efficiently than liquid fuel. On average, LPG, CNG, and gasoline produced 18.38, 19.57, and 15.83 % BTE. The CNG produced the highest BTE compared to gasoline and LPG. However, adding HHO further increases the BTE. On average, LPG-HHO and CNG-HHO produced 22.66 and 24.01 % higher BTE than gasoline. During the compression stroke, gasoline continues to vaporize. This lowers the temperature of the working charge, thereby lowering the compression work while simultaneously increasing the amount of vapor in the working charge. Thus, the cooling effect is insufficient to offset the impact caused by additional vapor due to lower latent heat in the case of gasoline. On the contrary, the higher latent heat of HHO blended fuel increases the cooling effect (i.e., reduces the compression work) [82]. Hence, BTE was higher in the case of LPG-HHO and CNG-HHO in the case of gasoline. BTE drops at lower load conditions due to the drop in the air-to-fuel ratio. The higher heating values that gaseous fuel possesses can be used to justify the rise in BTE for CNG fuel. In the engine inlet, CNG and air mix better than liquid fuel, which first atomizes and then evaporates to form the homogenous mixture, taking a comparatively longer time. Improved combustion results from a better air-to-fuel proportion for CNG and hydroxy mixture [48]. Çakmak et al. [54] reported an increase in BTE of 3.03 to 12.97 % for the LPG-HHO blended as the flow rate of HHO increased from 1 to 4 LPM. Falahat et al. [55] reported an increase of 14 to 23 % in BTE for gasoline and HHO blend. Jahirul et al. [78] reported a 1.6 % increase in BTE for CNG compared with gasoline.

Appendix briefly compares the engine performance parameters ascertained in the current study with the numerical findings of the previous research.

Exhaust emissions based on experimental approach

Fig. 6 depicts that gaseous fuel generates lower CO emissions than liquid fuel. On average, LPG and CNG produced 32.61 and 33.36 % lower CO emissions than gasoline (G). CO concentration rises due to incomplete combustion, and there is a direct relationship between incomplete combustion and CO content. The liquid fuels require more time to atomize and evaporate to generate a homogenous mixture with entering air, whereas the gaseous fuels mix well with air at the intake manifold. CO emission is influenced by the engine's fuel-to-air ratio, implying that a blend of HHO gas decreases the concentration of CO in the exhaust significantly by reducing gasoline fuel usage [70]. In gaseous fuels, improved mixture formation leads to improved combustion, reducing CO emission [83]. Adding HHO in LPG and CNG further

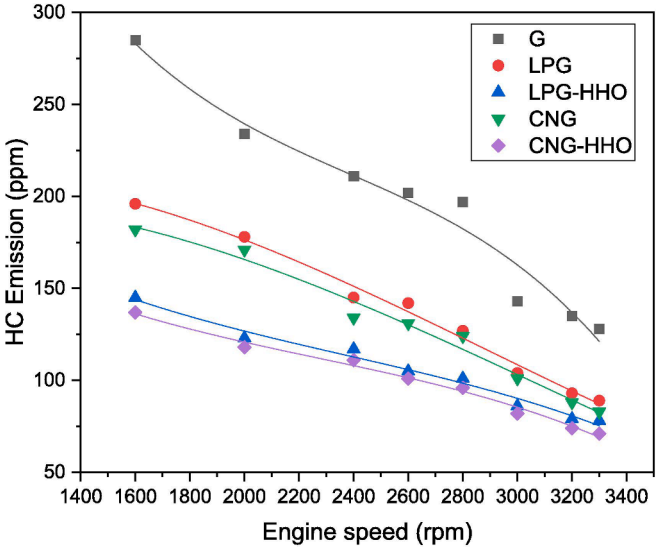

Fig. 7. Comparisons of HC emission at various engine speeds for gasoline, CNG, CNG-HHO, LPG, and LPG-HHO blend.

decreases the CO emission content by 14.96 % and 15.13 %, respectively. A greater hydrogen-to-carbon ratio is the cause of the decrease in CO concentrations for the HHO-CNG and HHO-LPG mixtures. Less carbon is present in the mix, which results in lower carbon-oxygen reaction percentages in the exhaust. Low CO concentrations result from the high hydrogen flame rate, lean engine operating conditions brought on by HHO, and enhanced combustion [84,85]. Simsek and Uslu [46] reported a 62.03 % decrease in CO emissions for LPG compared with gasoline. Jahirul et al. [78] reported a 45.55 % decrease in CO emissions for CNG compared with gasoline. EL-Kassaby et al. [70] reported an 18 % decrease in CO emissions for the HHO-gasoline fuel blend at an HHO flow rate of 18 LPH.

Gaseous fuels typically exhibit reduced HC emissions compared to gasoline, as depicted in Fig. 7. On average, LPG and CNG produced HC emissions 30.03 % and 33.94 % lower than gasoline (G). The diminished HC emissions associated with gaseous fuels stem from improved mixture formation in the intake pipe and decreased absorption and adsorption by lubricant oil films. LPG and CNG, possessing lower molecular weights than gasoline, uniformly combine with air and ignite more rapidly than liquid fuels, necessitating atomization and vaporization. This improved combustion process reduces HC emissions [27,86]. Furthermore, introducing HHO into LPG and CNG further reduces HC emissions by 15.64 % and 14.59 %, respectively. Hybrid blends involving HHO and other gaseous fuels consistently exhibit lower levels of unburned hydrocarbons than LPG, CNG, and gasoline, mirroring the trends observed in CO and CO_2 emissions. The decline in HC emissions can be attributed to the rapid ignition and enhanced diffusivity characteristic of HHO-LPG and HHO-CNG blends [84,85]. Çakmak et al. [54] reported a decrease of 4.6 to 21 % in HC emissions for LPG- HHO blends at variable HHO flow rate from 1 to 4 LPM. Simsek and Uslu [46] reported a decrease of 63 % for LPG compared with gasoline. Tabar et al. [87] reported a 50 % decrease in HC emissions for CNG in comparison with gasoline. Jahirul et al. [78] also observed a 22.14 % decrease in HC emissions for CNG compared with gasoline.

Fig. 8 presents the variations in CO_2 emissions across engine speeds ranging from 1600 to 3300 rpm. It is important to note that gaseous fuels yield lower CO_2 emissions than liquid fuels. On average, LPG and CNG produced CO_2 emissions 18.82 % and 16.34 % lower than gasoline (G). This discrepancy can be attributed to gaseous fuels' higher hydrogen and lower carbon content. Conversely, gasoline's higher carbon content generates more carbon dioxide due to larger carbon fractions [88]. Introducing HHO into LPG and CNG further reduces CO_2 emissions by 7.69 % and 8.2 %, respectively. Notably, incorporating HHO into LPG substantially decreases CO_2 emissions, primarily because the fuel predominantly comprises hydrogen. Additionally, the lower number of carbon atoms in gaseous fuels contributes to reduced CO_2 emissions compared to liquid fuels [30,89]. Simsek and Uslu [46] reported a 56.42 % decrease in CO_2 emissions for LPG at full-throttle conditions compared to gasoline. However, Hashem et al. [56] observed a 14.44 % decrease in CO_2 emissions for LPG compared with gasoline. Jahirul et al. [78] reported a 30.88 % decrease in CO_2 emissions compared to gasoline. Likewise, Yontar and Dogu [76] observed a 12.1 % decrease in CO_2 emissions for CNG compared with gasoline.

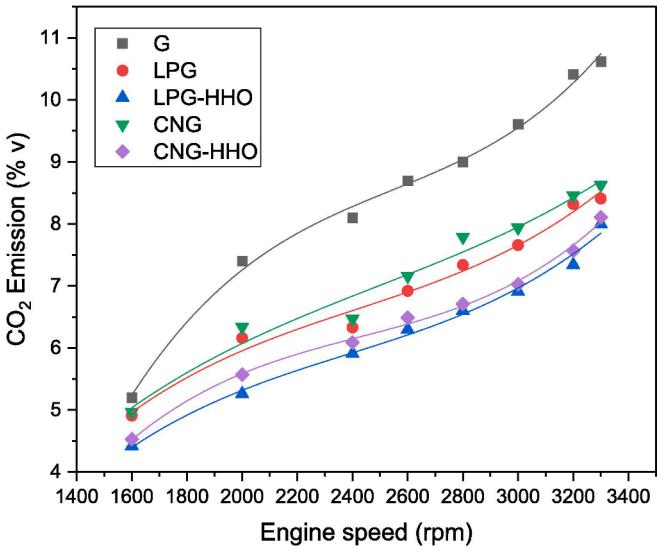

Fig. 8. Comparisons of CO_2 emission at various engine speeds for gasoline, CNG, CNG-HHO, LPG, and LPG-HHO blend.

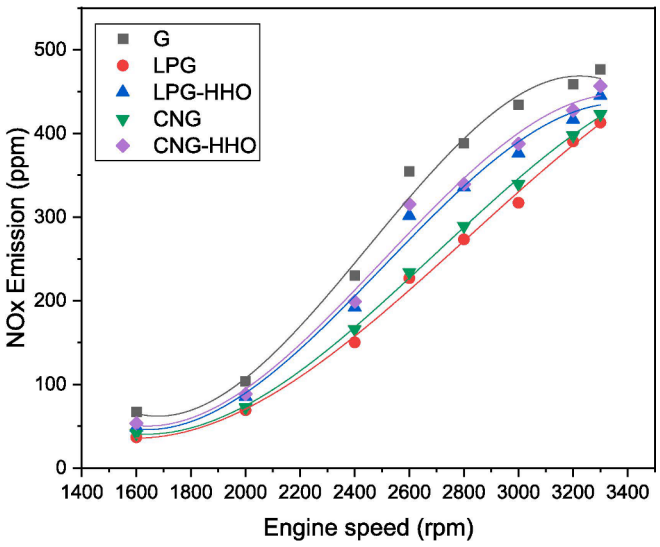

Fig. 9. Comparisons of NOx emission at various engine speeds for gasoline, CNG, CNG-HHO, LPG, and LPG-HHO blend.

Gaseous fuels generally exhibit lower NOx emissions than gasoline, as shown in Fig. 9. On average, LPG and CNG produced NOx emissions 25.36 % and 21.90 % lower than gasoline (G). NOx forms when a substantial quantity of air (N_2, O_2) ignites at exceedingly high temperatures within the cylinder. Elevated NOx emissions often result from excess available air and high flame temperatures. Introducing HHO into the intake duct reduces the gasoline ratio, creating a lean mixture and lowering the flame temperature, subsequently decreasing NOx emissions. HHO gas enhances combustion characteristics and diminishes fuel consumption across all speed ranges, leading to a downward shift in emission curves [70]. Reduced NOx emissions from gaseous fuels occur due to their displacement of the air approaching the combustion chamber, limiting nitrogen's availability to form NOx [90]. However, adding HHO to LPG and CNG increases NOx emissions by 12.92 % and 12.10 %, respectively. Contrary to standalone LPG and CNG, LPG-HHO and CNG-HHO blends produce higher NOx emissions when utilized in SI engines. Three significant factors contributing to NOx generation include the available burning time, the physical state of the fuel, the presence of oxygen and nitrogen, and the temperature within the combustion chamber. Therefore, the elevated combustion temperatures within engine cylinders resulting from the combustion of hydrogen fractions cause substantial NOx emissions from these blends [27,91,92]. Previous research has shown an increase in NOx emissions for LPG and CNG compared to gasoline. However, in the current research work, the NOx emissions for CNG and LPG decrease compared to gasoline. However, adding HHO in LPG and CNG is responsible for the increase in NOx

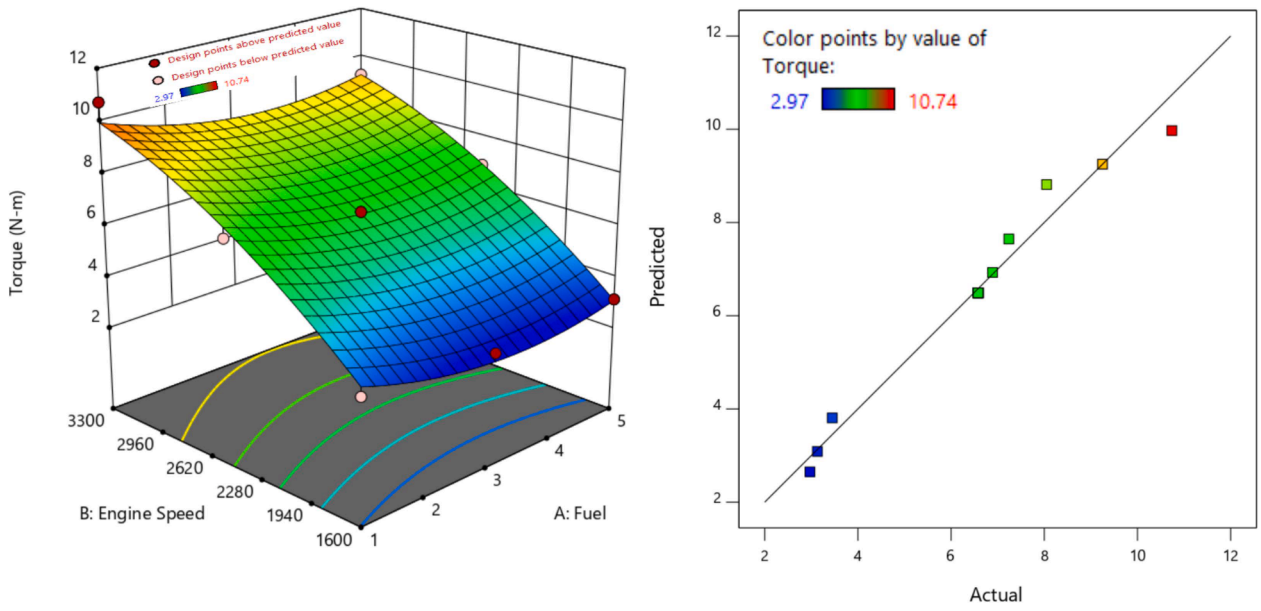

Fig. 10. (a) Response surface of torque, (b) Comparison of actual and predicted values of torque.

emissions compared with LPG and CNG alone. Çakmak et al. [54] reported an increase in NOx emissions of 2.22 to 6.42 % for LPG-HHO at a variable HHO flow rate of 1 to 4 LPM. EL-Kassaby et al. [70] reported a decrease in NOx emissions of 15 % for gasoline-HHO blend at HHO flow rate of 18 LPH. Hashem et al. [56] reported an 8 % increase in NOx emissions for LPG compared with gasoline. Yontar and Dogu [76] reported a 3.3 % increase in NOx emissions for CNG compared with gasoline. However, Jahirul et al. [78] observed a 50 % increase in NOx emissions for CNG compared with gasoline.

Appendix briefly compares the engine exhaust emission characteristics ascertained in the current study with the numerical findings of the previous research.

Central composite DOE

Central Composite Design of Experiments (CCDOE) is a highly adaptable and essential statistical approach that holds substantial importance for research and industrial applications. Its effectiveness stems from its comprehensive method of exploring the complex interplay between numerous input variables and their influence on a targeted result. RSM is a potent tool for optimizing complex systems by bridging the gap between cost and time, serving in extensive experimentation. In this section, the results present insights into the intricate relationships between variables and their potential for improvement. The predictive results provide a pathway to effective decision-making, operational enhancements, and a deeper understanding of the contributing factors.

Engine performance-based CCDOE approach

Fig. 10 (a) shows a performance analysis of an engine fueled with gasoline, LPG, LPG-HHO, CNG, and CNG-HHO in terms of torque. The results reveal distinct performance characteristics, where gasoline demonstrates robust power output with a torque of 10.74 Nm at 3300 rpm, highlighting its capacity for high torque generation. LPG-HHO exhibits competitive performance, portraying a balanced trade-off between power and efficiency across various engine speeds. CNG-HHO also demonstrates promising performance, particularly at 3300 rpm, suggesting the potential benefits of hydrogen-enhanced fuels on engine torque. The current dataset underscores the significant impact of fuel selection for investigating engine performance and presents implications for optimizing performance across various applications. Fig. 10 (b) compares actual and predicted torque values. The data points in the close vicinity of the regression line indicate the closeness between actual and predicted values. With an R^2 value of 0.9739, the statistical study shows an excellent model fit, which accounts for 97.39 % of the variation in the data. After regulating the predictors, the model's robustness is further supported by the adjusted R^2, which stands at 0.9608. Data variability is low, as seen by the low standard deviation (0.4493) and low coefficient of variation (CV%) of 6.90 %. Additionally, the adequate precision of 26.276 indicates a significant signal-to-noise ratio higher than the desired limit of greater than 4. It indicates the excellence of data fitting between predicted and experimental values.

Table 7 presents the ANOVA for the engine torque. The F-value (74.54) indicates the overall significance of the model, with a minimal likelihood of occurring by random chance ($p < 0.0001$), confirming its robustness in explaining torque's variation. Moreover, A-Fuel, B-Engine Speed, and their quadratic terms (A2 and B2) exhibit statistically significant effects, as evidenced by low p-values ($p < 0.05$), underscoring their considerable influence on torque. Conversely, a significant lack of

Table 7
ANOVA for torque.

Source	Sum of Squares	df	Mean Square	F-value	p-value		PC %
Model	60.18	4	15.04	74.54	< 0.0001	significant	97.3944
A-Fuel	0.7776	1	0.7776	3.85	0.0853		1.2585
B-Engine Speed	56.98	1	56.98	282.32	< 0.0001		92.2156
A^2	1.76	1	1.76	8.71	0.0184		2.8484
B^2	1.58	1	1.58	7.85	0.0231		2.5570
Residual	1.61	8	0.2018				2.6056
Lack of Fit	1.61	4	0.4036	4035.63	< 0.0001		2.6056
Pure Error	0.0004	4	0.0001				0.0006
Cor Total	61.79	12					

fit with an F-value of 4035.63 suggests an undesirable lack of fit of the model, emphasizing the need for further model refinement. This analysis provides a precise evaluation of the statistical significance and implications of various factors within the study, facilitating a deeper understanding of torque's behavior and the associated system dynamics. A statistical fit depicts how well a given statistical model conforms to the observed data, demonstrating how effectively the model can account for the deviations in the observed data. The p-value acts as a metric that indicates the probability of the null hypothesis to be true. Lower p-values indicate the strength of evidence against the null hypothesis. For ANOVA, the F-value comes into play and aids in determining a model's overall significance or the effect of a particular element. Larger F-values indicate a higher level of statistical significance. The lack of fit effectively evaluates the accuracy with which the statistical model describes the data by evaluating how closely the model's predictions align with the actual data points. A considerable lack of fit suggests a need to modify the model to reflect the data so that it can be analyzed more accurately. The model reflects the data well, as indicated by the lack of fit ($F = 4{,}035.63$, $p < 0.0001$), suggesting minimal unexplained variability. These findings validate the use of RSM in this research and demonstrate the robustness of our model, emphasizing its predictive power.

Equation (5) describes the relationship between torque and two input factors: fuel type (Fuel) and engine speed (Speed). It reveals that fuel type leads to reduced torque, while higher engine speeds have a positive impact, resulting in increased torque. The presence of quadratic terms for fuel and speed suggests optimal levels, with deviations from these optimal levels leading to diminished torque. Notably, as speed continues to increase beyond a certain point, torque experiences a decline. This equation provides valuable insights into the complex interactions between the system's fuel blend, speed, and torque, allowing for a nuanced understanding of how these variables influence the outcome.

$$\text{Torque} = 6.49 - 0.3600 \times \text{Fuel} + 3.08 \times \text{Speed} + 0.7976 \times \text{Fuel}^2 - 0.7574 \times \text{Speed}^2 \quad (5)$$

Fig. 11 (a) presents a comprehensive BP analysis in an engine employing five distinct fuel types: gasoline, LPG, LPG-HHO, CNG, and CNG-HHO. The notable observations include gasoline's robust BP performance, achieving 3.71 kW at 3300 rpm, highlighting its proficiency in generating high power output. At 2450 rpm, the engine fueled with gasoline produced a BP of 1.82 kW. However, LPG-HHO displays competitive BP attributes, ranging from 1.50 to 1.73 kW at varying engine speeds, underscoring a harmonious equilibrium between power and efficiency. Meanwhile, CNG-HHO exhibits promising BP performance, notably reaching 2.94 kW at 3300 rpm, implying the favorable impact of hydrogen-enriched fuels on BP. The findings accentuate the profound influence of fuel selection on BP, emphasizing gasoline's suitability for high-power applications and underscoring the competitive BP performance of LPG-HHO and CNG-HHO, particularly within the hydrogen-enriched fuel context. Fig. 11 (b) compares actual and predicted BP values. The model's statistical metrics reveal a good match, with an adjusted R^2 of 0.9787 suggesting robustness when predictors are taken into consideration and an R^2 of 0.9858 indicating that the model explains 98.58 % of the variance in the data. The data is stable around the mean of 1.76, as seen by the low standard deviation of 0.1385. An indicator of the model's dependability is adequate precision of 36.8643, which denotes a substantial signal-to-noise ratio. The consistency between the predicted R^2 and adjusted R^2 is emphasized in the remark, highlighting the model's power and appropriateness for real-world applications, notably in design space navigation.

Table 8 presents the ANOVA for the engine's BP. ANOVA analysis assesses how well the RSM model predicts BP. Moreover, factors like A-Fuel, B-Engine Speed, AB, and A2 emerged as significant contributors to the model's effectiveness, as reflected in their low p-values. A strong fit was shown by the model's total sum of squares of 10.65 and substantial F-value of 138.85 ($p < 0.0001$). In addition to the main effect of fuel type (A) with $F = 7.36$ ($p = 0.0266$), the main effect of engine speed (B) with $F = 532.97$ ($p < 0.0001$) was significant, along with the interaction effect (AB) with $F = 6.57$ ($p = 0.0334$) and the quadratic impact of fuel type (A2) with $F = 8.51$ ($p = 0.0194$). The model appears to reflect the data properly, as indicated by the lack of fit ($F = 478.30$, $p < 0.0001$), showing little unexplained variability. The noticeable significance of lack of fit, supported by an F-value of 478.30, with only a 0.01 % likelihood of occurring by random chance, underscores the importance of ensuring a well-fitting model. These statistical findings shed light on how different factors play their role in determining BP, emphasizing the importance of a well-tailored model in this context.

Equation (5) shows the relation between input and output parameters, such as how fuel blends and engine speed affect BP. Both linear and quadratic associations between fuel blends and engine speed with BP are

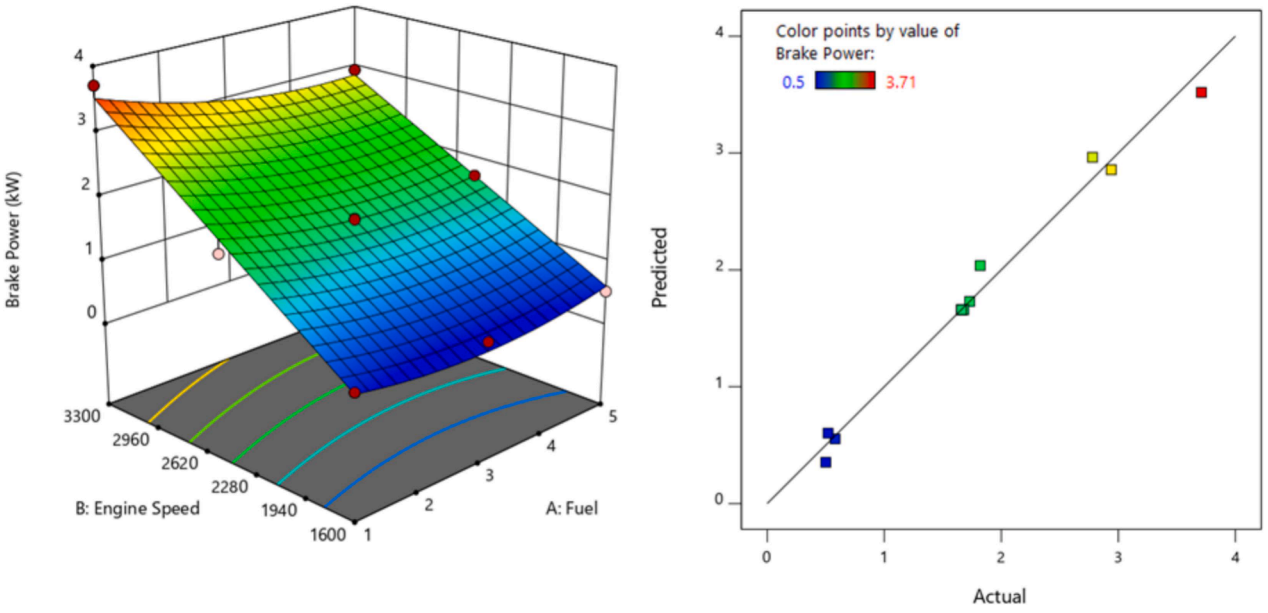

Fig. 11. (a) Response surface of BP (b) Comparison of actual and predicted BP values.

Table 8
ANOVA for BP.

Source	Sum of Squares	df	Mean Square	F-value	p-value		PC%
Model	10.65	4	2.66	138.85	< 0.0001	significant	98.6111
A-Fuel	0.1411	1	0.1411	7.36	0.0266		1.3065
B-Engine Speed	10.22	1	10.22	532.97	< 0.0001		94.6296
AB	0.1260	1	0.1260	6.57	0.0334		1.1667
A^2	0.1632	1	0.1632	8.51	0.0194		1.5111
Residual	0.1534	8	0.0192				1.4204
Lack of Fit	0.1531	4	0.0383	478.30	< 0.0001		1.4176
Pure Error	0.0003	4	0.0001				0.0028
Cor Total	10.80	12					

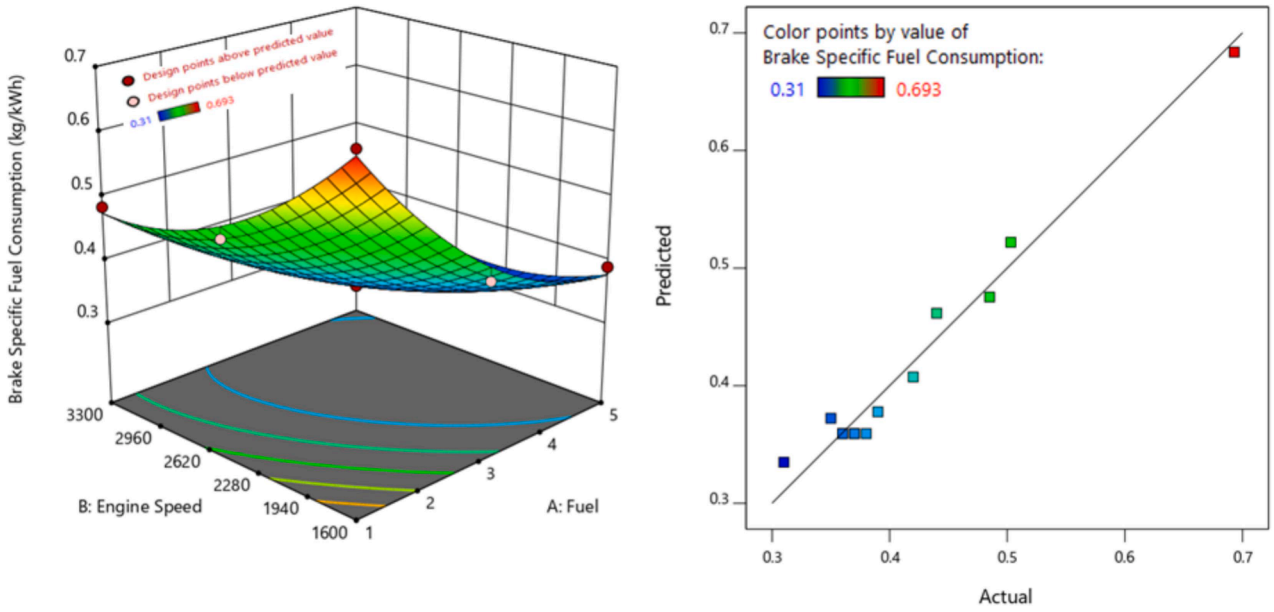

Fig. 12. (a) Response surface of BSFC (b) Comparison of actual and predicted BSFC values.

meticulously accounted for in equation (6). The assigned coefficients (−0.1533, 1.30, −0.1775, and 0.2248) signify the magnitude of influence each term exerts in the determination of BP. The model inherently investigates the intricate interplay between fuel and speed in shaping the resultant BP, thus acknowledging the potential presence of interactions and quadratic relationships.

$$\text{Brake Power} = 1.66 - 0.1533\text{xFuel} + 1.30\text{xSpeed} - 0.1775\text{xFuelxSpeed} + 0.2248\text{xFuel}^2 \quad (6)$$

Fig. 12 (a) illustrates the BSFC performance, employing gasoline, LPG, LPG-HHO, CNG, and CNG-HHO as fuel sources. Fig. 12 (a) highlights gasoline's commendable efficiency with a BSFC of 0.485 kg/kWh at 3300 rpm. Furthermore, it visually emphasizes LPG-HHO's competitive BSFC metrics, showcasing a harmonious equilibrium between power generation and fuel economy. Fig. 12 (a) shows varying values ranging from 0.36 to 0.44 kg/kWh at different engine speeds. Similarly, Fig. 12 (a) illustrates CNG-HHO's substantial BSFC of 0.42 kg/kWh at 3300 rpm, corroborating efficiency and commendable brake power. Notably, this efficiency extends to lower engine speeds, as signified by the graphical representation of an efficiency rate of 0.39 kg/kWh at 1600 rpm. Fig. 12(a) highlights the important function of fuel choice in controlling BSFC, especially in hydrogen-enriched fuels. This graphical depiction provides a clear road map for maximizing engine performance by finding the ideal ratio between fuel choice and BSFC for various applications. Fig. 12 (b) compares actual and predicted BSFC values. The coefficient of variation (CV%) at 5.03 % denotes low relative variability, while the standard deviation (Std. Dev.) of 0.0210 denotes

Table 9
ANOVA for BSFC.

Source	Sum of Squares	Df	Mean Square	F-value	p-value		PC%
Model	0.1146	5	0.0229	51.95	< 0.0001	significant	97.3662
A-Fuel	0.0525	1	0.0525	118.90	< 0.0001		44.6049
B-Engine Speed	0.0120	1	0.0120	27.13	0.0012		10.1954
AB	0.0142	1	0.0142	32.10	0.0008		12.0646
A^2	0.0132	1	0.0132	29.94	0.0009		11.2150
B^2	0.0092	1	0.0092	20.81	0.0026		7.8165
Residual	0.0031	7	0.0004				2.6338
Lack of Fit	0.0028	3	0.0009	13.37	0.0149		2.3789
Pure Error	0.0003	4	0.0001				0.2549
Cor Total	0.1177	12					

minimum data uncertainty compared to the Mean (0.4178). The model's capacity to explain a considerable amount (97.38 %) of the data variance is shown by the R^2 value of 0.9738. This is further supported by the adjusted R^2 value of 0.9550, which highlights the model's robustness in the context of predictor variables. In addition, despite a modest decline in predictive accuracy, the congruence between the predicted R^2 (0.8331) and the adjusted R^2 indicates the model's dependability. Indicating a strong signal-to-noise ratio above the minimum threshold of 4, the adequate precision ratio of 24.4454 confirms the model's suitability for studying design space and actual implementation.

Table 9 signifies the ANOVA for BSFC. ANOVA analysis is performed to assess how well the RSM model predicts BSFC. A strong fit is shown by the model's total sum of squares of 0.1146 and substantial F-value of 51.95 ($p < 0.0001$). In addition to the main effects of fuel type (A) with $F = 118.90$ ($p < 0.0001$) and engine speed (B) with $F = 27.13$ ($p = 0.0012$), the interaction effect (AB) with $F = 32.10$ ($p = 0.0008$), the quadratic impact of fuel type (A2) with $F = 29.94$ ($p = 0.0009$), and the quadratic impact of engine speed (B2) with $F = 20.81$ ($p = 0.0026$) were also significant. The model reflects the data properly, as indicated by the lack of fit ($F = 13.37$, $p = 0.0149$), and shows little unexplained variability. The overall model exhibits significant statistical relevance, as indicated by a substantial F-value of 51.95, with an exceptionally low 0.01 % likelihood of such an outcome occurring by random chance. Individual factors, namely A-Fuel, B-Engine Speed, AB, A2, and B2, emerge as highly significant contributors to the model's efficacy, supported by their lower p-values. Notably, the significance of lack of fit is also highlighted, substantiated by an F-value of 13.37, with a 1.49 % probability of occurring due to random chance. It underscores the imperative of establishing a well-fitted model in this analytical context. These statistically driven findings provide valuable insights into the multifaceted interplay of factors affecting BSFC, emphasizing the role of these factors and the critical importance of a precisely calibrated model.

Equation (7) indicates the quantitative assessment of BSFC. This model, designed carefully, emphasizes two pivotal variables (fuel and speed). It comprehensively accommodates linear and quadratic associations between these variables and the resultant BSFC, with the accompanying coefficients (−0.0935, −0.0447, 0.0595, 0.0692, and 0.0577) serving as precise measures of their respective contributions. This mathematical construct thus functions as a robust and sophisticated analytical instrument, facilitating an exhaustive exploration of the intricate interdependencies between fuel and speed, encompassing both linear and nonlinear relationships while characterizing the determinants of BSFC.

$$\mathrm{BSFC} = 0.3592 - 0.0935\mathrm{xFuel} - 0.0447\mathrm{xSpeed} + 0.0595\mathrm{xFuelxSpeed} + 0.0692\mathrm{xFuel}^2 + 0.0577\mathrm{xSpeed}^2 \quad (7)$$

Fig. 13 (a) shows BTE within the operational spectrum of an engine, focusing on five distinct fuel types: gasoline, LPG, LPG-HHO, CNG, and CNG-HHO. The results reveal that gasoline exhibits BTE, with a recorded value of 16.21 % at 3300 rpm, attesting to its capacity to efficiently convert fuel into useful work, albeit at a moderate level. The engine's consistent performance for gasoline fuel is further emphasized by a BTE of 15.63 % at 2450 rpm, indicating reliability across varying engine speeds. In contrast, LPG-HHO emerges as a remarkable contender, boasting BTE values ranging from 15.03 to 23.61 % at diverse engine speeds, thus signifying an equitable balance between power generation and fuel efficiency. Similarly, CNG-HHO showcases commendable BTE figures, attaining 23.61 % at 3300 rpm, thereby underscoring the positive influence of hydrogen-enriched fuels on BTE. The efficiency is not confined solely to higher engine speeds, as evidenced by a BTE of 15.19 % at 1600 rpm. These findings are paramount for optimizing engine performance and ensuring an equitable equilibrium between power output and judicious fuel utilization across various applications. Fig. 13 (b) compares actual and predicted BTE values. The R2 value, reaching 0.9940, accentuates the model's exceptional capacity to explicate a substantial proportion (99.40 %) of data variance, corroborated by the adjusted R2 value of 0.9897, affirming the model's robustness in the context of predictor variables. Furthermore, the congruence between the predicted R2 at 0.9406 and the adjusted R2 underscores the model's dependability, even when considering predictor variables. The adequate precision ratio, marked at 47.2088, substantially surpasses the requisite threshold of 4, signifying a robust signal-to-noise ratio and, thus, corroborating the model's reliability for design space exploration and real-world applications.

The analysis of BTE unveils statistical findings of remarkable significance, offering invaluable insights into the relationship between factors and the efficiency of the braking system. ANOVA assesses how well the RSM model predicts BTE. A strong fit was shown by the model's total sum of squares of 191.17 and substantial F-value of 231.75 ($p <$ 0.0001). In addition to the main effects of fuel type (A) with $F = 331.70$

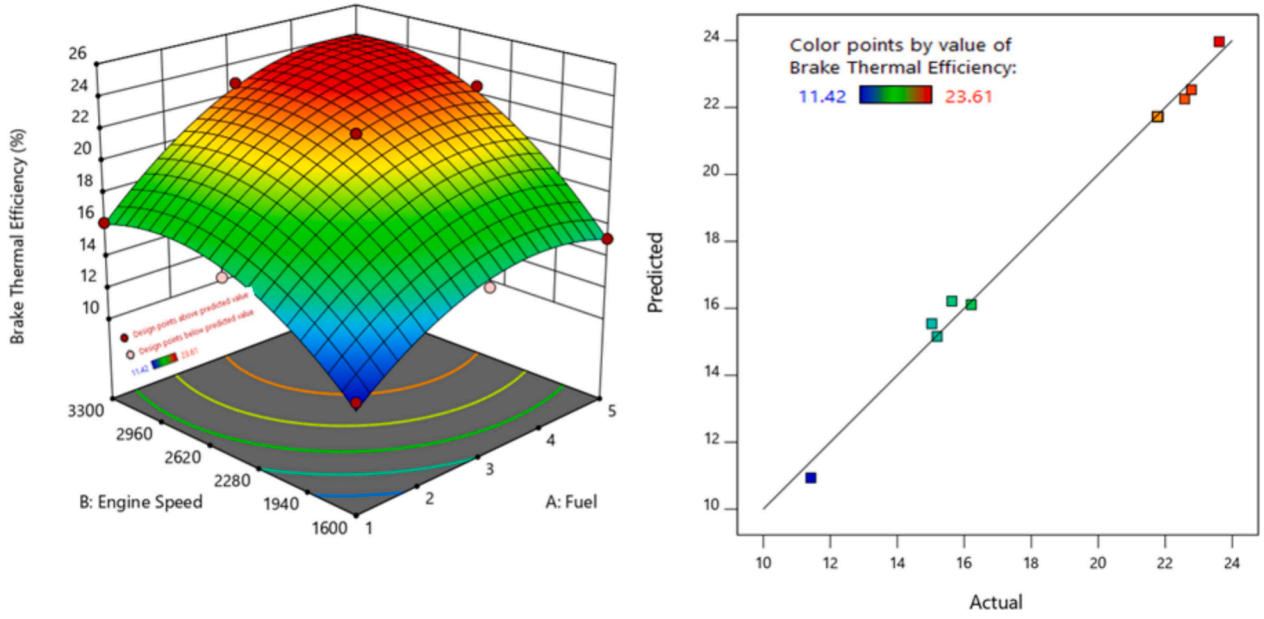

Fig. 13. (a) Response surface of BTE, (b) Comparison of actual and predicted values.

Table 10
ANOVA for BTE.

Source	Sum of Squares	df	Mean Square	F-value	p-value		PC%
Model	191.17	5	38.23	231.75	< 0.0001	significant	99.4020
A-Fuel	54.72	1	54.72	331.70	< 0.0001		28.4526
B-Engine Speed	73.22	1	73.22	443.83	< 0.0001		38.0720
AB	3.29	1	3.29	19.97	0.0029		1.7107
A^2	17.13	1	17.13	103.86	< 0.0001		8.9070
B^2	20.00	1	20.00	121.21	< 0.0001		10.3993
Residual	1.15	7	0.1650				0.5980
Lack of Fit	1.15	3	0.3848	2959.72	< 0.0001		0.5980
Pure Error	0.0005	4	0.0001				0.0003
Cor Total	192.32	12					

($p < 0.0001$) and engine speed (B) with $F = 443.83$ ($p < 0.0001$), the interaction effect (AB) with $F = 19.97$ ($p = 0.0029$), the quadratic impact of fuel type (A2) with $F = 103.86$ ($p < 0.0001$), and the quadratic impact of engine speed (B2) with $F = 121.21$ ($p < 0.0001$) were also significant. The model appears to properly reflect the data, as indicated by the lack of fit ($F = 2{,}959.72$, $p < 0.0001$), showing little unexplained variability. These findings validate the use of RSM in this research and show how robust our model is, emphasizing its predictive power. This underlines the model's strong explanatory power. Individual factors such as A-Fuel, B-Engine Speed, AB, A2, and B2 substantially contribute to the model's effectiveness, as their low p-values indicate. Their significance suggests that the type of fuel used and engine speed play pivotal roles in determining BTE. The significance of lack of fit, with an F-value of 2959.72, emphasizes the importance of obtaining a well-fitted model for accurate predictions. These findings shed light on the multifaceted dynamics affecting BTE and underscore the necessity for precise modeling, ultimately providing critical insights for optimizing braking system performance. Table 10 includes critical statistical metrics for a reduced quadratic model of brake thermal efficiency. The standard deviation (Std. Dev.) of 0.4062 highlights minimal data variance concerning the mean, which stands at 19.33, while the coefficient of variation (CV %) at 2.10 % indicates modest relative variability.

Equation (8) offers a comprehensive quantitative BTE computation framework. This thoughtfully constructed model considers two fundamental variables, fuel, and speed, and encompasses linear and quadratic associations between these variables and the ensuing BTE. The coefficients (−2.49, −2.69, 3.02, 3.49, and 0.9075) are instrumental in quantifying the magnitude and direction of their respective contributions. This mathematical construct is a robust analytical tool, facilitating an exhaustive exploration of the intricate interplay between fuel consumption and speed in shaping BTE, encompassing linear and nonlinear relationships.

$$\begin{aligned} BTE = {} & 21.72 + 3.02xFuel + 3.49xSpeed + \\ & 0.9075xFuelxSpeed - 2.49xFuel^2 - 2.69xSpeed^2 \end{aligned} \quad (8)$$

Exhaust emissions based on the CCDOE approach

Fig. 14 (a) thoroughly examines the engine's CO emissions fueled with the five distinct fuel variants: gasoline, LPG, LPG-HHO, CNG, and CNG-HHO. The results reveal that gasoline in the spectrum of CO emissions, from 1270 to 2876 ppm across varying engine speeds, indicates its inherent tendency to produce carbon monoxide, with lower emission levels observed at reduced speeds. Conversely, LPG-HHO maintains a notably consistent range of CO emissions, remaining within the narrow band of 723 to 725 ppm across differing engine speeds, suggesting stable emissions and potentially efficient combustion processes. In contrast, CNG-HHO demonstrates a broader spectrum of CO emissions, fluctuating between 701 and 1398 ppm, signifying varying emission levels contingent on engine speed variations. Such findings highlight the insightful influence of fuel choice on CO emissions, with gasoline contributing to higher emissions. However, LPG-HHO showcases consistent and relatively lower emissions, and CNG-HHO portrays a wider range of emissions levels. This insight contributes significantly to understanding the environmental implications of distinct fuel types and their potential for emissions reduction across diverse applications. Fig. 14 (b) compares actual and predicted CO

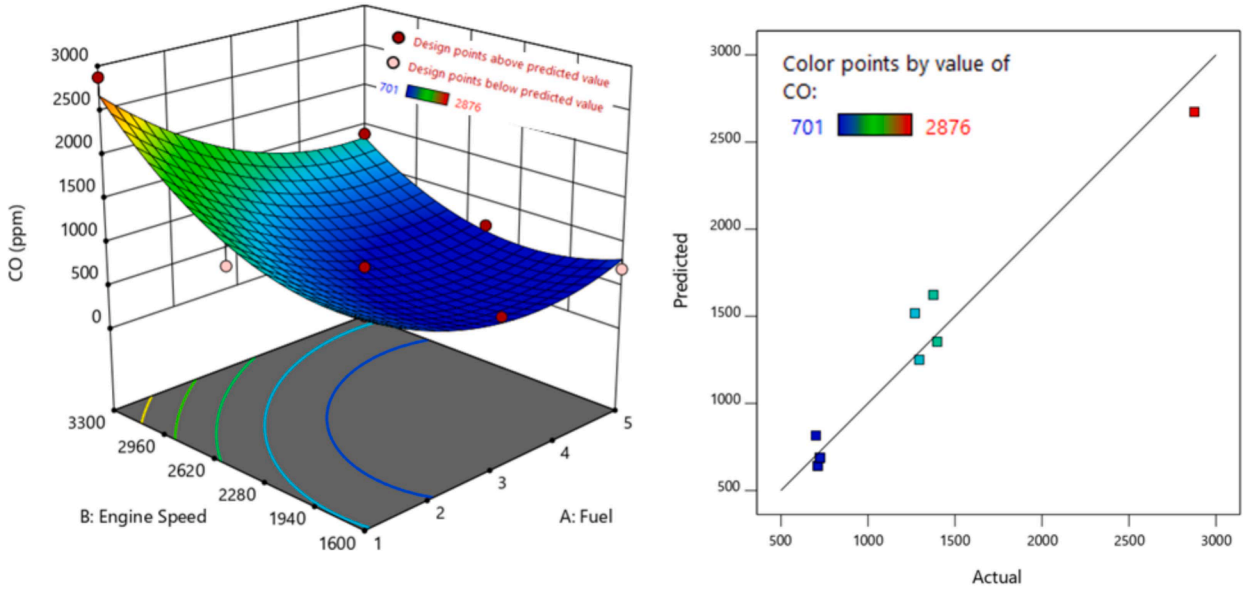

Fig. 14. (a) Response surface of CO (b) Comparison of actual and predicted CO values.

Table 11
ANOVA for CO emission.

Source	Sum of Squares	df	Mean Square	F-value	p-value		PC%
Model	4.349E + 06	5	8.699E + 05	30.98	0.0001	significant	95.6665
A-Fuel	1.154E + 06	1	1.154E + 06	41.09	0.0004		25.3850
B-Engine Speed	1.443E + 06	1	1.443E + 06	51.38	0.0002		31.7422
AB	1.954E + 05	1	1.954E + 05	6.96	0.0335		4.2983
A^2	4.215E + 05	1	4.215E + 05	15.01	0.0061		9.2719
B^2	5.449E + 05	1	5.449E + 05	19.41	0.0031		11.9864
Residual	1.965E + 05	7	28076.33				4.3225
Lack of Fit	1.965E + 05	3	65510.50	93586.43	< 0.0001		4.3225
Pure Error	2.80	4	0.7000				0.00006
Cor Total	4.546E + 06	12					

values. The considerable standard deviation (Std. Dev.) of 167.56 suggests a pronounced level of data dispersion around the mean of 1073.69. The coefficient of variation (CV %) at 15.61 % denotes a moderate degree of relative variability. The R2 value of 0.9568 underscores the model's capacity to elucidate a substantial share (95.68 %) of data variance, further validated by the adjusted R2 of 0.9259, emphasizing the model's stability in relation to predictor variables. However, a noticeable discrepancy arises between the predicted R2 at 0.5935 and the adjusted R2 at 0.9259, surpassing the customary threshold of 0.2. This divergence may indicate the presence of a significant block effect or potential concerns with the model or data, such as model simplification, response transformation, or the influence of outliers. Therefore, it is advisable to undertake confirmation runs to authenticate the model's performance. On a favorable note, the adequate precision ratio at 17.8549 signifies a robust signal-to-noise ratio, affirming the model's utility for effective navigation within the design space.

Table 11 displays the ANOVA for CO emission with fuel blend variation, which significantly impacts engine performance as its percentage contribution is 25.38 %. The analysis of CO emissions delivers profound statistical significance, yielding invaluable insights into the determinants of CO emissions. The substantial F-value of 30.98 for the overall model attests to its robust explanatory capacity, with a mere 0.01 % likelihood of such results occurring randomly. This underscores the model's strong predictive power. ANOVA is performed to assess how well the RSM model predicts CO emissions. A strong fit was shown by the model's total sum of squares of 4,349,000.00 and substantial F-value of 30.98 (p = 0.0001). In addition to the main effects of fuel type (A) with F = 41.09 (p = 0.0004) and engine speed (B) with F = 51.38 (p = 0.0002), the interaction effect (AB) with F = 6.96 (p = 0.0335), the quadratic impact of fuel type (A2) with F = 15.01 (p = 0.0061), and the quadratic impact of engine speed (B2) with F = 19.41 (p = 0.0031) were also significant. The model reflects the data properly, as indicated by the lack of fit (F = 93,586.43, p < 0.0001), showing little unexplained variability. These findings validate the RSM predicted CO emissions. The key factors, including A-Fuel, B-Engine Speed, AB, A2, and B2, emerge as highly significant influencers of CO emissions, as manifested by their impressively lower p-values. The pronounced significance of lack of fit, supported by an F-value of 93586.43 and a 0.01 % probability of random occurrence, accentuates the imperative of a meticulously tailored model for accurate CO emission predictions. These findings unravel the intricate interplay of factors impacting CO emissions, emphasizing the need for precise modeling to comprehend CO emission dynamics comprehensively. Ultimately, this underscores the significance of these insights in guiding efforts to manage and reduce CO emissions effectively.

This mathematical model thoroughly considers two pivotal variables (fuel and speed). Equation (9) accommodates both linear and quadratic associations between these variables and the variable CO, with the accompanying coefficients (−438.50, 490.33, −221.00, 390.67, and 444.17) serving to signify the magnitude and direction of their respective contributions quantitatively. This mathematical construct serves as a robust analytical instrument, facilitating a comprehensive exploration of the intricate interplay between fuel consumption and speed and their combined influence on CO while characterizing the determinants of this variable.

$$CO = 688.38 - 438.50xFuel + 490.33xSpeed - 221.00xFuelxSpeed + 390.67xFuel^2 + 444.17xSpeed^2 \quad (9)$$

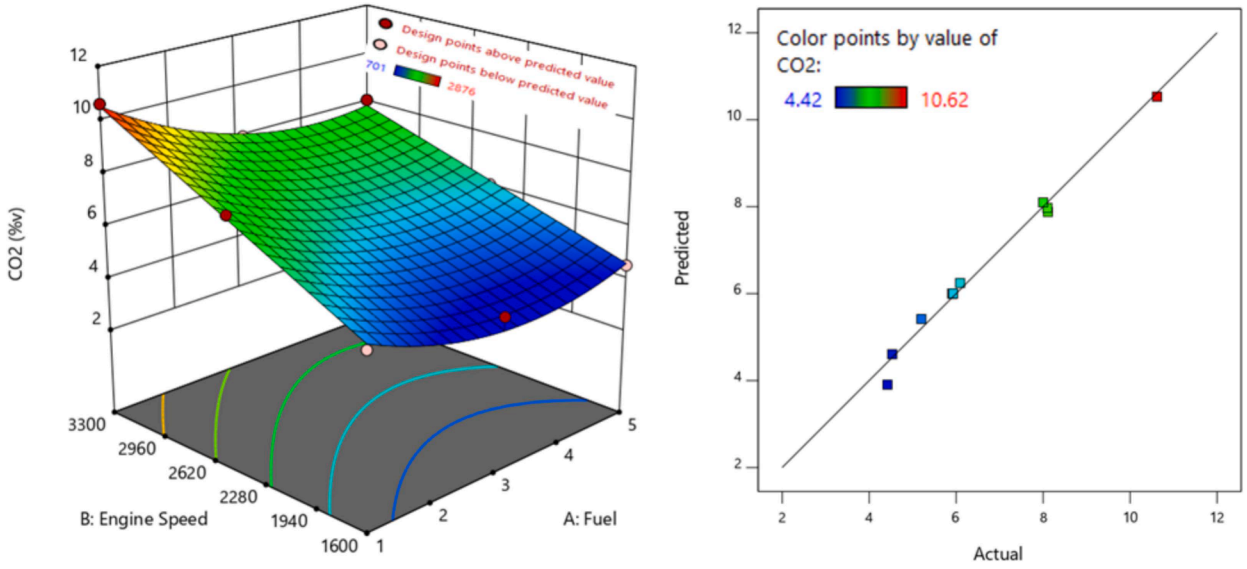

Fig. 15. (a) Response surface of CO_2, (b) Comparison of actual and predicted CO_2 values.

Table 12
ANOVA for CO_2 emission.

Source	Sum of Squares	df	Mean Square	F-value	p-value		PC%
Model	35.67	4	8.92	153.90	< 0.0001	significant	98.7268
A-Fuel	4.49	1	4.49	77.48	< 0.0001		12.4273
B-Engine Speed	26.38	1	26.38	455.20	< 0.0001		73.0141
AB	0.8464	1	0.8464	14.61	0.0051		2.3427
A^2	3.96	1	3.96	68.32	< 0.0001		10.9604
Residual	0.4636	8	0.0579				1.2831
Lack of Fit	0.4633	4	0.1158	1654.54	< 0.0001		1.2823
Pure Error	0.0003	4	0.0001				0.0008
Cor Total	36.13	12					

Fig. 15 (a) illustrates an engine's CO_2 emissions utilizing five distinct fuel types: gasoline, LPG, LPG-HHO, CNG, and CNG-HHO. The graphical representation depicts gasoline resulting in a range of CO_2 emissions, from 5.2 to 10.62 %v, at various engine speeds, with a discernible increase in emissions at higher speeds. In contrast, Fig. 15 (a) illustrates that LPG-HHO maintains a relatively moderate CO_2 emission profile, hovering within the narrow band of 4.42 to 8.11 %v at varying engine speeds, signifying stable emissions. Furthermore, Fig. 15 (a) represents CNG-HHO as exhibiting a broader span of CO_2 emissions, fluctuating between 4.53 and 8.11 %v, as variations influenced by engine speed. These graphical insights provide a clear visual narrative of the environmental impact of different fuel types and their potential role in reducing CO_2 emissions in diverse applications. Fig. 15 (b) compares actual and predicted CO_2 values. The standard deviation (Std. Dev.) is relatively low at 0.2407, suggesting minimal variation around the mean of 6.51. The coefficient of variation (CV %) is 3.70 %, indicating a low level of relative variability. The R2 value is 0.9872, indicating that the model explains a substantial portion (98.72 %) of the variance in the data, with an adjusted R2 of 0.9808, signifying the model's robustness while accounting for predictor variables. Importantly, the predicted R2 (0.9298) closely aligns with the adjusted R2 (0.9808), which is less than the typical threshold of 0.2, indicating a reliable model fit. Additionally, the adequate precision ratio of 44.3796 significantly exceeds the desired threshold 4, affirming a strong signal-to-noise ratio. Given its strong statistical performance, this model is well-suited for navigating the design space or practical applications.

The CO_2 emissions reveal statistically significant insights, shedding light on the intricate web of factors that drive CO_2 emissions within the study's specific context. The notable F-value of 153.90 for the overall model underscores its robust capacity for prediction, with an exceptionally low 0.01 % probability of these results occurring randomly (see Table 12). ANOVA is performed to assess how well the RSM model predicts CO_2 emissions. A strong fit was shown by the model's total sum of squares of 35.67 and substantial F-value of 153.90 ($p < 0.0001$). In addition to the main effects of fuel type (A) with $F = 77.48$ ($p < 0.0001$) and engine speed (B) with $F = 455.20$ ($p < 0.0001$), the interaction effect (AB) with $F = 14.61$ ($p = 0.0051$) and the quadratic impact of fuel type (A2) with $F = 68.32$ ($p < 0.0001$) were also significant. The model appears to properly reflect the data, as indicated by the lack of fit ($F = 1{,}654.54$, $p < 0.0001$), showing little unexplained variability. These findings validate the RSM predicted results regarding CO_2 emissions and show the robustness of the model. Critical factors such as A-Fuel, B-engine speed, AB, and A^2 emerge as influential drivers of CO_2 emissions, exemplified by their impressively low p-values. The noteworthy significance of lack of fit, confirmed by an F-value of 1654.54 and a 0.01 % probability of random occurrence, accentuates the necessity for a meticulously calibrated model to ensure accurate CO_2 emissions forecasts. These findings provide pivotal insights into the multifaceted interactions shaping CO_2 emissions, emphasizing the critical role of precise modeling in gaining a holistic understanding of CO_2 emission dynamics. Ultimately, these insights are pivotal in guiding strategies for effective CO_2 emissions management and reduction.

Equation (10) represents a mathematical model for estimating CO_2 emissions based on fuel and speed variables. This model includes both linear and quadratic relationships between these variables and CO_2. Each coefficient (−0.8650, 2.10, −0.4600, and 1.11) quantifies the impact and direction of its respective variable on CO_2 emissions. Considering both linear and nonlinear dependencies, the equation

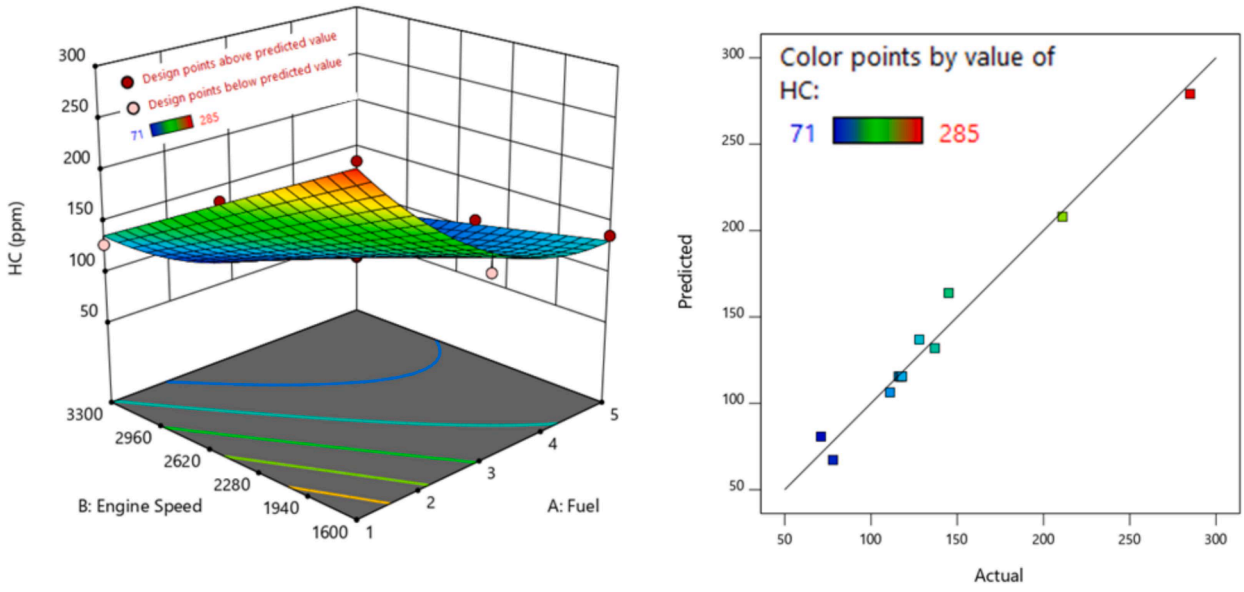

Fig. 16. (a) Response surface of HC emission, (b) Comparison of actual and predicted HC values.

allows for a detailed examination of how fuel type and speed interact and collectively influence CO_2 emissions.

$$CO_2 = 6.00 - 0.8650xFuel + 2.10xSpeed - 0.4600xFuelxSpeed + 1.11xFuel^2 \quad (10)$$

Fig. 16 (a) illustrates the HC emissions derived from the engine operations over a well-defined speed range, encompassing five distinct fuel compositions, i.e., gasoline, LPG, LPG-HHO, CNG, and CNG-HHO. The observations indicate that gasoline results in a range of HC emissions, spanning from 128 to 285 ppm at varying engine speeds, thereby signifying the production of hydrocarbons, notably elevated at higher engine speeds. In contrast, LPG-HHO maintains a relatively consistent and modest HC emission profile, fluctuating within the confined range of 116 to 145 ppm across diverse engine speeds, indicating a steady and controlled pattern of HC emissions. Conversely, CNG-HHO presents a broader spectrum of HC emissions, oscillating between 71 and 137 ppm while showing the lowest maximum emission value. These empirical insights underscore the substantial impact of fuel selection on HC emissions, with gasoline contributing to a varied range of emissions, LPG-HHO maintaining a relatively steady and moderate emission pattern, and CNG-HHO showcasing emissions variations tied to engine speed. The CNG-HHO blend considerably emerges with the lowest emissions among the five fuels, emphasizing its potential to reduce HC emissions across different applications. These findings bear significance in unraveling the environmental implications associated with diverse fuel types and their potential role in minimizing HC emissions. Fig. 16 (b) displays the relation between actual and predicted values with the standard deviation (Std. Dev.) at a moderate level of 9.72, indicating some variation around the mean of 134.77. The coefficient of variation (CV %) at 7.21 % suggests a moderate degree of relative variability. The R2 value of 0.9801 underscores the model's capacity to explain a substantial portion (98.01 %) of data variance, with the adjusted R2 of 0.9701 reaffirming the model's stability, particularly considering predictor variables. Significantly, the predicted R2 (0.8721) closely aligns with the adjusted R2 (0.9701), with a difference of less than 0.2, attesting to a reliable model fit. Furthermore, the adequate precision ratio of 35.1515 greatly exceeds the recommended threshold of 4, affirming a robust signal-to-noise ratio. Given its robust statistical performance and reliability, this model is well-suited for design space exploration applications.

The analysis of HC emissions reveals statistically significant insights, offering a valuable understanding of the intricate factors influencing HC emissions, as displayed in Table 14. ANOVA is performed to assess how well the RSM model predicts HC emissions. A strong fit was shown by the model's total sum of squares of 37,180.84 and substantial F-value of 98.43 ($p < 0.0001$). In addition to the interaction effect (AB) with $F = 21.92$ ($p = 0.0016$) and the quadratic impact of fuel type (A2) with $F = 59.19$ ($p < 0.0001$), the main effects of fuel type ($F = 164.18$, $p < 0.0001$) and engine speed ($F = 148.43$, $p < 0.0001$) were also significant. The model appears to reflect the data properly, as indicated by the lack of fit ($F = 268.81$, $p < 0.0001$), showing little unexplained variability. The substantial F-value of 98.43 for the overall model underscores its robust predictive capacity, with an exceedingly low 0.01 % likelihood of these results occurring randomly. This highlights the model's substantial explanatory prowess. The significant factors, including A-Fuel, B-Engine Speed, AB, and A2, emerge as influential drivers of HC emissions, as demonstrated by their considerably lower p-values. The significance of lack of fit, supported by an F-value of 268.81 and a 0.01 % probability of random occurrence, accentuates the necessity for a meticulously calibrated model to ensure accurate HC emissions forecasts. These findings furnish indispensable insights into the intricate interplay of factors shaping HC emissions, underscoring the critical role of precise modeling in gaining a comprehensive understanding of HC emission dynamics and crafting effective emissions control and reduction strategies.

Equation (11) presents a mathematical model for calculating HC emissions based on two primary variables: fuel and speed. This model considers linear and quadratic relationships between these variables and HC emissions. Each coefficient (−50.83, −48.33, 22.75, and 41.60) represents the magnitude and direction of its respective influence on HC emissions. This equation allows for a detailed analysis of how fuel consumption and speed interact and collectively affect HC emissions, encompassing linear and nonlinear relationships.

$$HC = 115.57 - 50.83xFuel - 48.33xSpeed + 22.75xFuelxSpeed + 41.60xFuel^2 \quad (11)$$

Fig. 17 (a) shows NOx emissions from the engine fueled with five distinct fuel compositions, i.e., gasoline, LPG, LPG-HHO, CNG, and CNG-HHO. The gasoline yields a range of NOx emissions, spanning from 67.2 to 476.6 ppm across diverse engine speeds, signifying the production of nitrogen oxides, considerably escalating with increasing engine speeds. In contrast, LPG-HHO maintains a relatively consistent and modest NOx emission profile, fluctuating within the constrained range of 48.7 to 199.1 ppm at varying engine speeds, signifying a steady and controlled

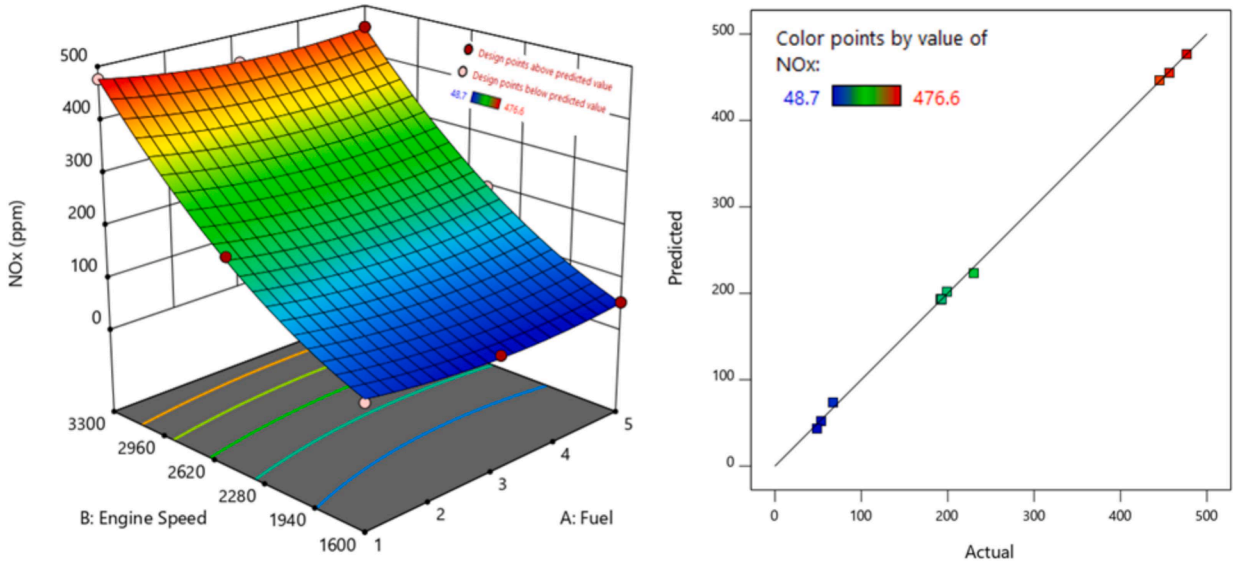

Fig. 17. (a) Response surface of NOx, (b) Comparison of actual and predicted NOx values.

Table 13
ANOVA for HC emission.

Source	Sum of Squares	df	Mean Square	F-value	p-value		PC%
Model	37180.84	4	9295.21	98.43	< 0.0001	significant	98.0086
A-Fuel	15504.17	1	15504.17	164.18	< 0.0001		40.8689
B-Engine Speed	14016.67	1	14016.67	148.43	< 0.0001		36.9479
AB	2070.25	1	2070.25	21.92	0.0016		5.4572
A^2	5589.76	1	5589.76	59.19	< 0.0001		14.7346
Residual	755.46	8	94.43				1.9914
Lack of Fit	752.66	4	188.17	268.81	< 0.0001		1.9840
Pure Error	2.80	4	0.7000				0.0074
Cor Total	37936.31	12					

Note: Table 5 twice remain all renumbered citation also changed kindly check.

Table 14
ANOVA for NOx emissions.

Source	Sum of Squares	df	Mean Square	F-value	p-value		PC%
Model	2.568E + 05	4	64190.27	3885.96	< 0.0001	significant	99.9611
A-Fuel	695.53	1	695.53	42.11	0.0002		0.2707
B-Engine Speed	2.437E + 05	1	2.437E + 05	14750.35	< 0.0001		94.8618
A^2	1051.70	1	1051.70	63.67	< 0.0001		0.4094
B^2	7429.12	1	7429.12	449.75	< 0.0001		2.8918
Residual	132.15	8	16.52				0.0514
Lack of Fit	131.48	4	32.87	196.83	< 0.0001		0.0512
Pure Error	0.6680	4	0.1670				0.0003
Cor Total	2.569E + 05	12					

pattern of NOx emissions. Conversely, CNG-HHO exhibits a broader spectrum of NOx emissions, oscillating between 53.5 and 456.7 ppm, underscoring the discernible influence of engine speed on NOx production. These empirical insights underscore the profound impact of fuel selection on NOx emissions, with gasoline contributing to a diverse range of emissions, LPG-HHO sustaining a relatively stable and moderate emission pattern, and CNG-HHO manifesting emissions variations associated with engine speed. These findings are paramount for discerning the environmental implications of distinct fuel types and their potential to mitigate NOx emissions across diverse applications. Fig. 17 (b) depicts the relation between actual and predicted values with the data points scattered near the regression line. The standard deviation (Std. Dev.) is considerably low at 4.06, denoting minimal data variability around the mean of 226.05. The coefficient of variation (CV %) at 1.80 % signifies exceptional data consistency and precision. The R2 value of 0.9995 indicates that the model elucidates an overwhelming majority (99.95 %) of data variance. The adjusted R2 of 0.9992 underscores the model's resilience, even when accommodating predictor variables. Moreover, the predicted R2 (0.9979) aligns closely with the adjusted R2 (0.9992), with a disparity of less than 0.2, affirming a superior model fit. The adequate precision ratio, positioned at an exceptional 171.91, greatly exceeds the requisite threshold of 4, confirming a strong signal-to-noise ratio. This model is exceptionally well-suited for tasks involving design space exploration or practical applications due to its exceptional statistical performance and unwavering reliability.

The investigation of NOx emissions presents a compelling statistical narrative, offering profound insights into the influential factors dictating NOx emissions within the specific research framework. Table 13 depicts the ANOVA for a reduced quadratic model of NOx emissions. ANOVA is performed to assess how well the RSM model predicts NOx emissions. A strong fit was shown by the model's total sum of squares of 256,800.00 and substantial F-value of 3,885.96 ($p < 0.0001$). In addition to the main effects of fuel type (A) with $F = 42.11$ ($p = 0.0002$) and engine speed (B) with $F = 14{,}750.35$ ($p < 0.0001$), the quadratic impact of fuel type (A2) with $F = 63.67$ ($p < 0.0001$) and the quadratic impact of engine speed (B2) with $F = 449.75$ ($p < 0.0001$) were also significant. The model appears to properly reflect the data, as indicated by the lack of fit ($F = 196.83$, $p < 0.0001$), depicting little unexplained variability. The substantial F-value of 3885.96 for the overall model underscores its robust predictive capability, with an exceptionally low 0.01 % probability of these results occurring randomly. The key factors, including A-Fuel, B-Engine Speed, A2, and B2, emerge as significant drivers of NOx emissions, as demonstrated by their impressively low p-values. The significance of lack of fit, supported by an F-value of 196.83 and a 0.01 % probability of random occurrence, underscores the need for a meticulously tailored model to ensure accurate NOx emissions forecasts. These findings provide valuable insights into the intricate interplay of factors shaping NOx emissions, emphasizing the pivotal role of precise modeling in achieving a comprehensive understanding of NOx emission dynamics and formulating effective emissions control and reduction strategies.

Equation (12) provides a mathematical model for estimating NOx emissions. It considers two important variables (fuel and speed) and incorporates linear and quadratic relationships between them and NOx emissions. Each coefficient (−10.77, 201.52, 19.51, and 51.86) quantifies the magnitude and direction of its respective impact on NOx emissions. This model offers a structured framework for exploring how fuel consumption and speed interact and jointly influence NOx emissions, covering both linear and nonlinear aspects of their relationship.

$$\mathrm{NOx} = 193.11 - 10.77\mathrm{xFuel} + 201.52\mathrm{xSpeed} + 19.51\mathrm{xFuel}^2 + 51.86\mathrm{xSpeed}^2 \quad (12)$$

RSM based optimization

RSM-based optimization is mainly responsible for optimizing a system or process by setting multiple objectives and targets. This method uses mathematical models to understand and manipulate the relationships between input factors and desired output variables, identifying optimal conditions for achieving multiple outcomes like maximum power, minimum fuel consumption, maximum BTE, and minimum exhaust emissions. The optimization process has yielded precise engine operational parameters, revealing that the optimal configuration entails an engine speed of 2758 rpm and CNG-HHO, thereby endorsing the suitability of CNG-HHO fuel for this particular engine setup. The comprehensive analysis of these optimal settings was conducted through various response variables, encompassing pivotal performance indicators, including 7.94452 Nm for torque and 2.13813 kW for BP

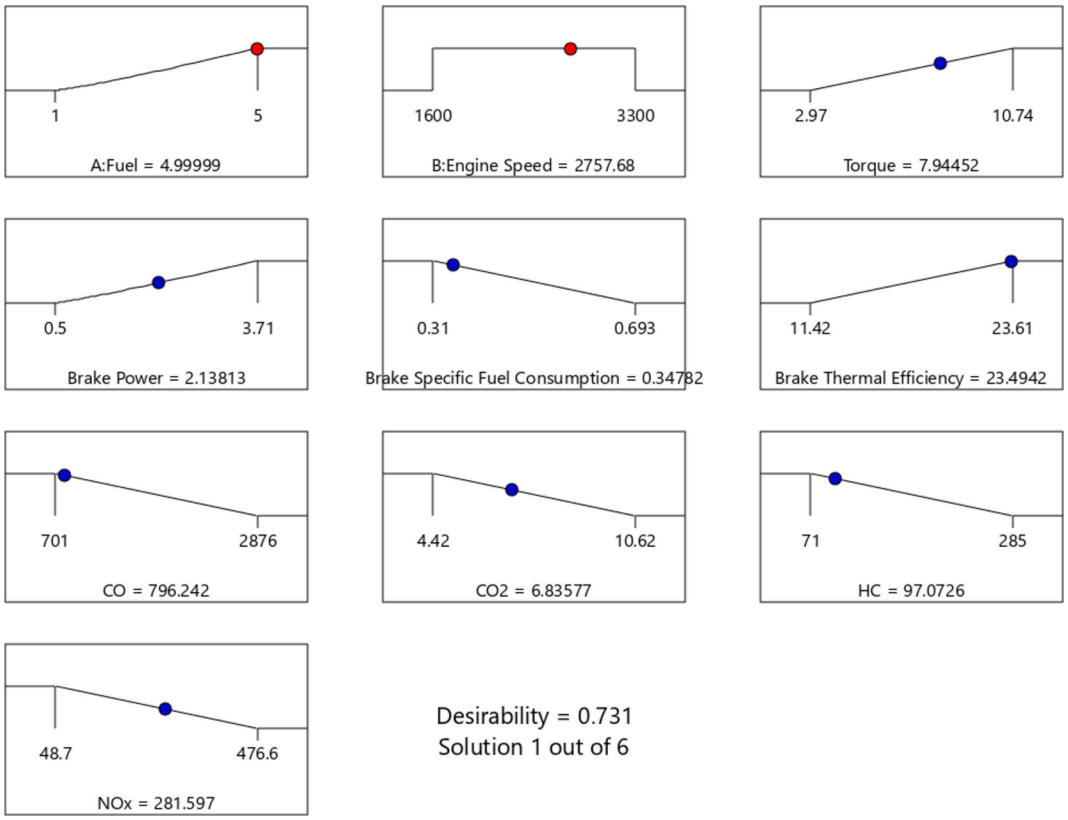

Fig. 18. RSM predicted optimized results.

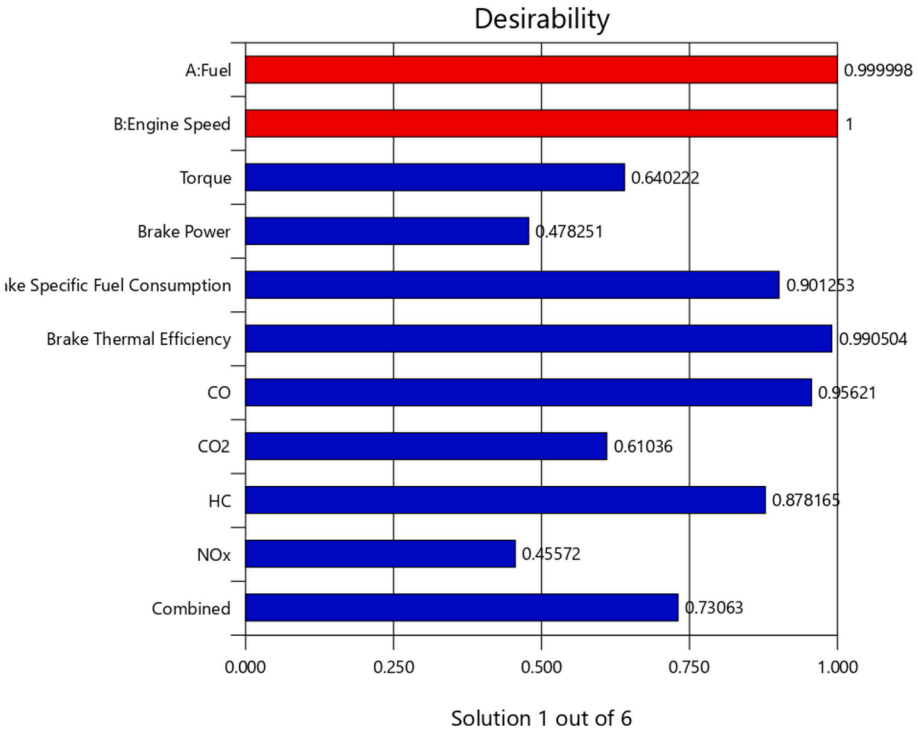

Fig. 19. Desirability chart.

thereby underscoring substantial mechanical enhancements. Furthermore, the pronounced achievement of a BTE of 23.4942 % and the concurrent realization of a BSFC of 0.34782 kg/kWh underscore the salient attributes of engine efficiency under these conditions.

The current study also delved into the emission aspects, demonstrating notable reductions in NOx emissions, registering 281.597 ppm, as well as a decrease in HC emissions, measuring 97.0726 ppm, along with CO_2 emissions at 6.83577 %v. Nevertheless, observing a slight

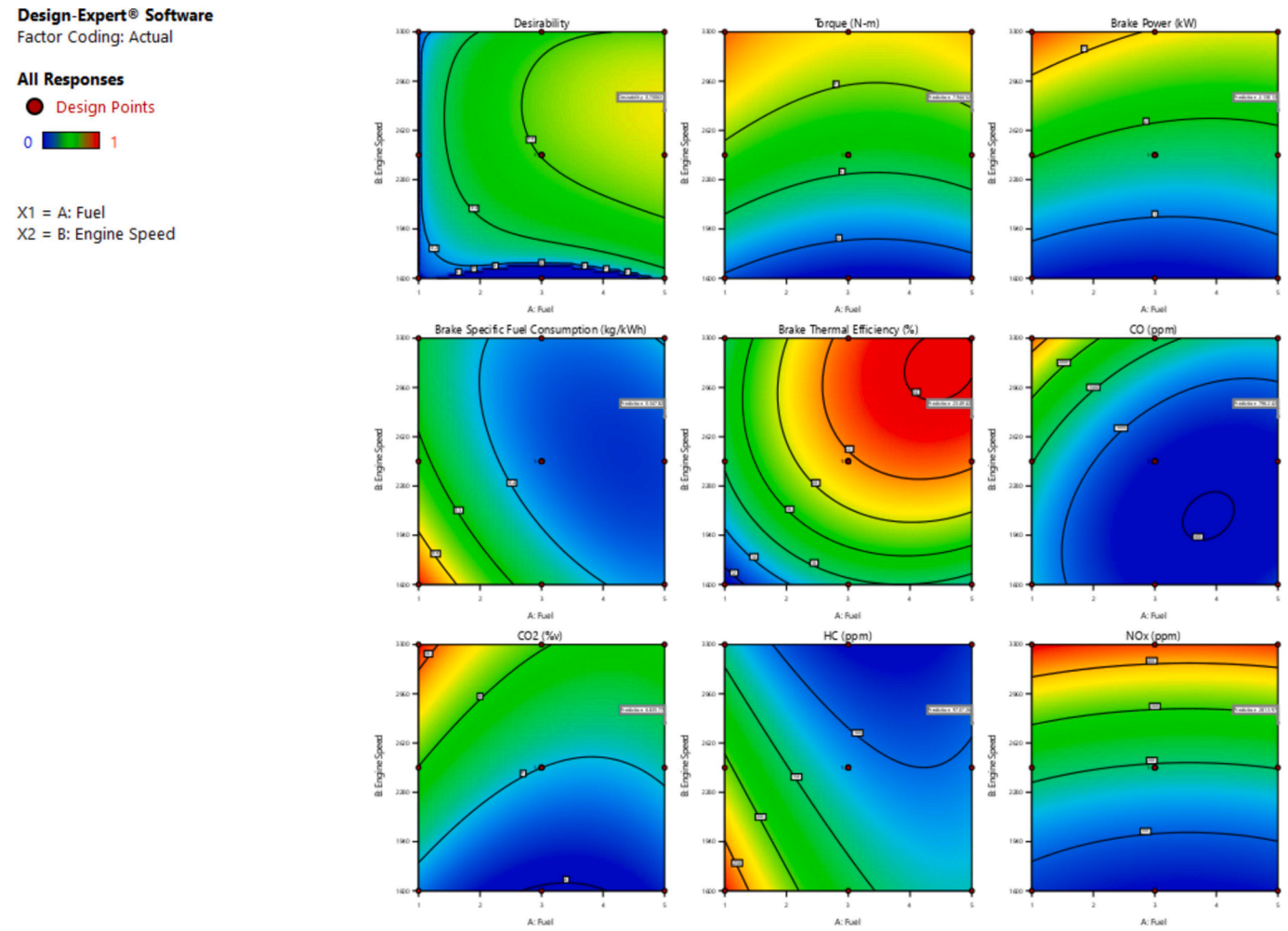

Fig. 20. Contour plots of all responses.

increase in CO emissions, peaking at 796.242 ppm, suggests a nuanced trade-off. The graphical representation of these optimal values in Fig. 18, symbolized by the utilization of red and blue data points, underscores their pivotal significance within the broader dataset. The results underscore the potential of HHO-enriched CNG fuel as a promising avenue for enhancing engine performance while mitigating emissions, constituting a significant stride toward realizing environmentally responsible and efficient engine operation. However, it is imperative to acknowledge the inherent variability among different fuel blends, thereby highlighting the demand for precision in selecting specific operational conditions and fuel compositions to realize the intended enhancements in engine efficiency and emissions abatement, thus underscoring the intricate interplay of diverse factors implicated in the realm of engine optimization.

Additionally, to gain a deeper understanding of the influence of each individual response variable on the overall configuration, a bar graph, as depicted in Fig. 19, portrays the desirability chart. It highlights the individual desirability index denoted as 'd' and the combined desirability index denoted as 'D'. Desirability is a statistical and mathematical concept used to improve response variables simultaneously. This metric usually ranges from 0 to 1, where 0 represents a poor result (significantly departing from the intended target), and 1 represents an excellent result (achieving the particular goal). Combining several response variables into a single metric using desirability functions makes determining the best set of factor values easier. Desirability is most prominent for BTE at 0.990, signifying a highly favorable impact. At the same time, it has the lowest value for NOx emissions at 0.455, indicating a comparatively lesser desirability.

In Fig. 20, the contour analysis that explains the effect of five distinct fuels, labeled as gasoline (fuel 1), LPG (fuel 2), LPG-HHO (fuel 3), CNG (fuel 4), and CNG-HHO (fuel 5), on various engine performance parameters and emissions. The results unveil interesting insights into the relationship between fuel selection and engine characteristics. Considerably, the desirability index witnesses a substantial ascent with fuel 5 (CNG-HHO) utilization, as graphically depicted in the contour plots. Torque performance, crucial in engine dynamics, reaches its peak with fuel 1 (gasoline) and second maximum with fuel 5 (CNG-HHO). Similarly, the contour plots underscore that fuel 1 (gasoline) excels in generating maximum BP. A notable trend emerges as one transitions from fuel 1 to fuel 5, with BSFC consistently diminishing. Fuel 5 (CNG-HHO) stands out as the paragon of efficiency in fuel utilization. Further examination reveals that fuel 5 (CNG-HHO) has the highest BTE, denoting its ability to convert energy effectively. On the emissions front, fuel 5 (CNG-HHO) employment correlates with the lowest CO emissions, reflecting its environmental compatibility. CO_2 and HC emissions also display a decreasing trend from fuel 1 to fuel 5, with fuel 5 outperforming in emission reduction. The NOx emissions increase as one progresses from fuel 1 to fuel 5, with fuel 5 registering the highest NOx emissions, indicating a trade-off that must be considered alongside its other performance attributes. In summary, these contour plots in Fig. 20 offer a comprehensive depiction of fuel effects on engine performance and emissions, making it evident that the choice of fuel should be guided by specific performance and environmental criteria, with fuel 5 (CNG-HHO) emerging as a noteworthy candidate for a balanced compromise.

Conclusions

This study evaluates the emission and performance characteristics of SI engines using both conventional (gasoline) and non-conventional fuels (LPG, CNG, and HHO) to reduce the power gap between gasoline and gaseous fuels. Key findings include:

- HHO-LPG blend increased BP by 6 % compared to standalone LPG, while LPG's BSFC increased by 30 %. CNG produced 4.76 % higher torque than LPG, with HHO helping to balance torque across fuel types.
- LPG-HHO and CNG-HHO blend produced slightly lower torque than gasoline (16.77 % and 11.25 % lower, respectively), but achieved higher BTE, with averages of 18.38 % (LPG), 19.57 % (CNG), and 15.83 % (gasoline).
- When HHO was integrated with LPG and CNG, HC and CO_2 emissions were reduced. HC emissions dropped by 15.64 % and 15.59 %, while CO_2 emissions decreased by 7.69 % and 8.2 %. Conversely, incorporating HHO in the blending of LPG and CNG led to a decline in CO_2, CO, and unburned hydrocarbon emissions by approximately 14.96 % and 15.13 %, respectively.
- LPG and CNG exhibited, on average, 14.67 % and 25.67 % lower BSFC than gasoline.
- LPG and CNG demonstrated 25.36 % and 21.90 % lower NOx emissions than gasoline. However, adding HHO in LPG and CNG increased the NOx emission content by 12.92 % and 12.10 %, respectively. Notably, LPG-HHO and CNG-HHO blends exhibited higher NOx emissions than standalone LPG and CNG when employed in SI engines.
- RSM predicted results with an overall desirability of 0.731, identifying optimized parameters for a CNG-HHO fuel blend at an engine speed of 2757 rpm. Under such ideal conditions, the engine demonstrated a brake torque of 7.94 Nm, BP of 2.14 kW, BSFC of 0.35 kg/kWh, BTE of 23.5 %, CO of 796.24 ppm, CO_2 of 6.84 %v, HC of 97.07 ppm, and NOx of 281.6 ppm.
- The CNG-HHO blend outperformed CNG and LPG alone, offering higher BTE, improved BSFC, and lower emissions, making it a viable alternative to gasoline. Exhaust gas recirculation, selective catalyst reduction, and de-NOx technologies could mitigate elevated NOx emissions due to hydrogen's combustion temperature.

CRediT authorship contribution statement

Muhammad Ali Ijaz Malik: Writing – review & editing, Writing – original draft, Visualization, Validation, Software, Methodology, Investigation, Formal analysis, Data curation, Conceptualization. **Adeel Ikram:** Writing – review & editing, Writing – original draft, Visualization, Supervision, Software, Resources, Project administration, Methodology, Investigation, Formal analysis, Conceptualization. **Shayan Sohail:** Writing – review & editing, Writing – original draft, Visualization, Investigation. **Muhammad Naqvi:** Writing – review & editing. **Muhammad Khubaib:** Writing – review & editing. **Fayaz Hussain:** Writing – review & editing, Supervision, Resources. **Bo Zhang:** Writing – review & editing, Supervision, Resources.

Declaration of competing interest

The authors declare that they have no known competing financial interests or personal relationships that could have appeared to influence the work reported in this paper.

Appendix

Table 1-A
Comparison between current study and previous research results.

Authors	Fuel type	Engine specifications	Engine Performance	Exhaust Emissions
Çakmak et al. [54]	LPG, gasoline and HHO (1, 2, and 4 LPM)	661.5 cc single-cylinder SI engine	BP (1.24–5.04 %)↑BSFC (2.92 – 11.17 %)↓BTE (3.03 – 12.97 %)↑	CO (2.26–8.72 %)↓ HC (4.6 % – 21 %)↓NOx (2.22–6.42 %)↑
Yilmaz [41]	Diesel and HHO (5 LPM)	3567 cc water cooled CI engine	Torque (19.1 %)↑BSFC (14 %)↓	HC (5 %)↓CO (13.5 %)↓
EL-Kassaby et al. [70]	Gasoline and HHO (18 LPH)	1289 cc four-cylinder SI engine	BSFC (34 %)↓BTE (10 %)↑	CO (18 %)↓HC (14 %)↓NOx (15 %)↓
Falahat et al. [55]	Gasoline and HHO (1 – 2 LPM)	197 cc single-cylinder SI engine	Torque (1 – 12.6 %)↑SFC (2.9 – 16.9 %)↓BTE (14 – 23 %)↑	CO↓ NOx↓
Rajaram et al [93]	Diesel and HHO (1 – 3.3 LPM)	Single-cylinder CI engine with 5.9 kW rated power	BTE (11.06 %)↑BSFC (9.96 %)↓	CO (15.38 %)↓HC (18.18 %)↓ CO_2 (6.06 %)↑NOx (11.19 %)↑
Sherman and Pratap [94]	Gasoline and HHO (2 – 3 LPM)	Six-cylinder 3500 cc CI engine	BSFC (11 %)↓	CH_4 (69 %)↓HC (72 %)↓ CO_2 (13 %)↓NOx (48 %)↓
Simsek and Uslu [46]	Gasoline and LPG at full throttle opening	Single Cylinder 389 cc SI engine	BSFC (34.19 %)↑BTE (8.95 %)↑	CO (62.03 %)↓HC (63 %)↓ CO_2 (56.42 %)↓
Hashem et al [56]	Gasoline and LPG	Single-cylinder SI engine with 2.02 kW output power	BTE (4.52 %)↓BSFC (5.42 %)↓VE (4.65 %)↓	CO (11.54 %)↓ CO_2 (14.44 %)↓NOx (8 %)↑
Jahirul et al [78]	Gasoline and CNG	1594 cc four-cylinder SI engine	BP (19.25 %)↓BSFC (15.96)↓BTE	CO_2 (30.88)↓CO (45.55 %)↓HC

(continued on next page)

Table 1-A (*continued*)

Authors	Fuel type	Engine specifications	Engine Performance	Exhaust Emissions
			(1.6 %)↑EGT (24.21 %)↑	(22.14 %)↓NOx (50 %)↑
Yontar and Dogu [76]	Gasoline and CNG	1339 cc four-cylinder SI engine	Torque (12.7 %)↓BP (12.4 %)↓BSFC (16.5 %)↓	CO (89.7 %)↓ CO_2 (12.1 %)↓NOx (3.3 %)↑
Tabar et al [87]	Gasoline and CNG	1650 cc turbo-charged SI engine	BSFC (16 %)↓	CO (66 %)↓HC (50 %)↓
Current Study				
	LPG	219 cc single-cylinder SI engine	Torque (22.60 %)↓BP (23.67 %)↓BSFC (14.67 %)↓ BTE (16.11 %)↑	CO (32.61 %)↓ CO_2 (18.82 %)↓ HC (30.03 %)↓NOx (25.36 %)↓
	LPG-HHO		Torque (16.77 %)BP (17.10 %)BSFC (30.44)BTE (22.66 %)	CO (47.47 %) CO_2 (26.54 %)HC (45.67 %)NOx (12.44 %)
	CNG		Torque (18.19 %)↓BP (18.91 %)↓BSFC (25.67 %)↓BTE (23.63 %)↑	CO (33.36 %)↓ CO_2 (16.34 %)↓HC (33.94 %)↓NOx (21.90 %)↓
	CNG-HHO		Torque (11.25 %)↓BP (12.59 %)↓BSFC (35.70 %)↓BTE (24.01 %)↑	CO (48.49 %)↓ CO_2 (24.54 %)↓HC (48.53 %)↓NOx (9.8 %)↓

Data availability

Data will be made available on request.

References

[1] Ijaz Malik MA, et al. Response surface methodology application on lubricant oil degradation, performance, and emissions in SI engine: A novel optimization of alcoholic fuel blends. Sci Prog 2023;106(1):00368504221148342.

[2] K. Hashimoto, "Current situation of energy consumption and carbon dioxide emissions of our world," in *Global carbon dioxide recycling*: Springer, 2019, pp. 25-31.

[3] Khalife E, Tabatabaei M, Demirbas A, Aghbashlo M. Impacts of additives on performance and emission characteristics of diesel engines during steady state operation. Prog Energy Combust Sci 2017;59:32–78.

[4] G. Yun-shan, A. Shah, H. Chao, and A. Baluch, "Effect of biodiesel on the performance and combustion parameters of a turbocharged compression ignition engine," *Pakistan Journal of Engineering and Applied Sciences,* 2016.

[5] Malaquias ACT, Netto NAD, Filho FAR, da Costa RBR, Langeani M, Baêta JGC. The misleading total replacement of internal combustion engines by electric motors and a study of the Brazilian ethanol importance for the sustainable future of mobility: A review. J Braz Soc Mech Sci Eng 2019;41:1–23.

[6] Schifter I, González U, Díaz L, Sánchez-Reyna G, Mejía-Centeno I, González-Macías C. Comparison of performance and emissions for gasoline-oxygenated blends up to 20 percent oxygen and implications for combustion on a spark-ignited engine. Fuel 2017;208:673–81.

[7] Chen W-C, Tsai I-C, Chou K-W. Life-cycle cost analysis in determining an importance factor for fire department buildings. J Chin Inst Eng 2013;36(8):1029–44.

[8] Malik MAI, Usman M, Bashir R, Hanif MS, Zubair SWH. Use of methanol-gasoline blend: A comparison of SI engine characteristics and lubricant oil condition. J Chin Inst Eng 2022;45(5):402–12.

[9] Klepeis NE, et al. The National Human Activity Pattern Survey (NHAPS): A resource for assessing exposure to environmental pollutants. J Eposure Sci Environ Epidemiol 2001;11(3):231–52.

[10] Farooq M, Almustapha MN, Imran M, Saeed M, Andresen JM. In-situ regeneration of activated carbon with electric potential swing desorption (EPSD) for the H2S removal from biogas. Bioresour Technol 2018;249:125–31.

[11] A. Kak, N. Kumar, B. Singh, S. Singh, and D. Gupta, "Comparative study of emissions and performance of hydrogen boosted SI engine powered by gasoline methanol blend and gasoline ethanol blend," SAE Technical Paper, 0148-7191, 2015.

[12] Wang T, Yu W, Liu F, Fang M, Farooq M, Luo Z. Enhanced CO2 absorption and desorption by monoethanolamine (MEA)-based nanoparticle suspensions. Ind Eng Chem Res 2016;55(28):7830–8.

[13] Marshall JD, Behrentz E. Vehicle self-pollution intake fraction: children's exposure to school bus emissions. Environ Sci Tech 2005;39(8):2559–63.

[14] Banković-Ilić IB, Stamenković OS, Veljković VB. Biodiesel production from non-edible plant oils. Renew Sustain Energy Rev 2012;16(6):3621–47.

[15] Göktaş M, Balki MK, Sayin C, Canakci M. An evaluation of the use of alcohol fuels in SI engines in terms of performance, emission and combustion characteristics: A review. Fuel 2021;286:119425.

[16] Huang Y, Surawski NC, Zhuang Y, Zhou JL, Hong G. Dual injection: An effective and efficient technology to use renewable fuels in spark ignition engines. Renew Sustain Energy Rev 2021;143:110921.

[17] Sharma H, Dhir A, Mahla SK. Application of clean gaseous fuels in compression ignition engine under dual fuel mode: A technical review and Indian perspective. J Clean Prod 2021;314:128052.

[18] Amirante R, et al. Effects of natural gas composition on performance and regulated, greenhouse gas and particulate emissions in spark-ignition engines. Energ Conver Manage 2017;143:338–47.

[19] Korakianitis T, Namasivayam A, Crookes R. Natural-gas fueled spark-ignition (SI) and compression-ignition (CI) engine performance and emissions. Prog Energy Combust Sci 2011;37(1):89–112.

[20] Almustapha MN, Farooq M, Mohammed ML, Farhan M, Imran M, Andresen JM. Modification of acidic and textural properties of a sulphated zirconia catalyst for efficient conversion of high-density polyethylene into liquid fuel. Environ Sci Pollut Res 2020;27:55–65.

[21] Almustapha MN, Farooq M, Andresen JM. Sulphated zirconia catalysed conversion of high density polyethylene to value-added products using a fixed-bed reactor. J Anal Appl Pyrol 2017;125:296–303.

[22] Erkuş B, Sürmen A, Karamangil MI. A comparative study of carburation and injection fuel supply methods in an LPG-fuelled SI engine. Fuel 2013;107:511–7.

[23] M. Usman and N. Hayat, "Use of CNG and Hi-octane gasoline in SI engine: a comparative study of performance, emission, and lubrication oil deterioration," *Energy Sources, Part A: Recovery, Utilization, and Environmental Effects,* pp. 1-15, 2019.

[24] Singh AP, Pal A, Agarwal AK. Comparative particulate characteristics of hydrogen, CNG, HCNG, gasoline and diesel fueled engines. Fuel 2016;185:491–9.

[25] Huang X, Wang Y, Xing Z, Du K. Emission factors of air pollutants from CNG-gasoline bi-fuel vehicles: Part II. CO, HC and NOx. Sci Total Environ 2016;565:698–705.

[26] Mohamed ES. Experimental study on the effect of active engine thermal management on a bi-fuel engine performance, combustion and exhaust emissions. Appl Therm Eng 2016;106:1352–65.

[27] Usman M, et al. Use of gasoline, LPG and LPG-HHO blend in SI engine: A comparative performance for emission control and sustainable environment. Processes 2020;8(1):74.

[28] Lata D, Misra A, Medhekar S. Effect of hydrogen and LPG addition on the efficiency and emissions of a dual fuel diesel engine. Int J Hydrogen Energy 2012;37(7):6084–96.

[29] Subramanian B, Ismail S. Production and use of HHO gas in IC engines. Int J Hydrogen Energy 2018;43(14):7140–54.

[30] Usman M, Hayat N, Bhutta MMA. SI engine fueled with gasoline, CNG and CNG-HHO blend: comparative evaluation of performance, emission and lubrication oil deterioration. J Therm Sci 2021;30:1199–211.

[31] Usman M, et al. Enviro-economic assessment of HHO–CNG mixture utilization in spark ignition engine for performance and environmental sustainability. Energies 2022;15(21):8253.

[32] Ogunkoya D, Roberts WL, Fang T, Thapaliya N. Investigation of the effects of renewable diesel fuels on engine performance, combustion, and emissions. Fuel 2015;140:541–54.

[33] S. Wierzbicki, K. Duda, and M. Mikulski, "Renewable Fuels for Internal Combustion Engines," vol. 14, ed: MDPI, 2021, p. 7715.
[34] Ardebili SMS, Solmaz H, İpci D, Calam A, Mostafaei M. A review on higher alcohol of fusel oil as a renewable fuel for internal combustion engines: Applications, challenges, and global potential. Fuel 2020;279:118516.
[35] F. Ma *et al.*, "Performance and emission characteristics of a turbocharged spark-ignition hydrogen-enriched compressed natural gas engine under wide open throttle operating conditions," *international journal of hydrogen energy,* vol. 35, no. 22, pp. 12502-12509, 2010.
[36] Ma F, Wang Y, Ding S, Jiang L. Twenty percent hydrogen-enriched natural gas transient performance research. Int J Hydrogen Energy 2009;34(15):6523–31.
[37] Sekar D, Venkadesan G, Panithasan MS. Optimisation of dry cell electrolyser and hydroxy gas production to utilise in a diesel engine operated with blends of orange peel oil in dual-fuel mode. Int J Hydrogen Energy 2022;47(6):4136–54.
[38] Vimalananth V, Panithasan MS, Venkadesan G. Investigating the effects of injection and induction modes of hydrogen addition in a CRDI pilot diesel-fuel engine with exhaust gas recirculation. Int J Hydrogen Energy 2022;47(53):22559–73.
[39] Muthusamy J, Venkadesan G, Panithasan MS. Use of La2O3 with 8YSZ as thermal barrier coating and its effect on thermal cycle behavior, microstructure, mechanical properties and performance of diesel engine operated by hydrogen-algae biodiesel blend. Int J Hydrogen Energy 2022;47(63):27199–222.
[40] Nabil T, Dawood MMK. Enabling efficient use of oxy-hydrogen gas (HHO) in selected engineering applications; transportation and sustainable power generation. J Clean Prod 2019;237:117798.
[41] A. C. Yilmaz, E. Uludamar, and K. Aydin, "Effect of hydroxy (HHO) gas addition on performance and exhaust emissions in compression ignition engines," *international journal of hydrogen energy,* vol. 35, no. 20, pp. 11366-11372, 2010.
[42] N. K. Balakrishnan, P. Chelladorai, and Y. H. Teoh, "A Review on Hydroxy Gas Enrichment for Internal Combustion Engines," *SAE International Journal of Engines,* vol. 15, no. 03-16-06-0044, 2022.
[43] Santilli RM. A new gaseous and combustible form of water. Int J Hydrogen Energy 2006;31(9):1113–28.
[44] Demirbas A. Current Advances in Alternative Motor Fuels. Energy Explor Exploit 2003;21(5):475–87. https://doi.org/10.1260/014459803322986295.
[45] E. U. Ali Can Yilmaz, Kadir Aydin, "Effect of hydroxy (HHO) gas addition on performance and exhaust emissions in compression ignition engines," *International Journal of Hydrogen Energy,* vol. Volume 35, no. 20, pp. ages 11366-11372, 11 August 2010., doi: https://doi.org/10.1016/j.ijhydene.2010.07.040.
[46] Simsek S, Uslu S. Investigation of the impacts of gasoline, biogas and LPG fuels on engine performance and exhaust emissions in different throttle positions on SI engine. Fuel 2020;279:118528.
[47] Yontar AA, Doğu Y. Investigation of the effects of gasoline and CNG fuels on a dual sequential ignition engine at low and high load conditions. Fuel 2018;232:114–23.
[48] Duc KN, Duy VN, Hoang-Dinh L, Viet TN, Le-Anh T. Performance and emission characteristics of a port fuel injected, spark ignition engine fueled by compressed natural gas. Sustainable Energy Technol Assess 2019;31:383–9.
[49] P. Ouellette, B. Douville, P. Hill, and B. Ursu, "NOx reduction in a directly injected natural gas engine," in *Proceedings of the 1998 Fall Technical Conference of the ASME, IC Engines Division, ICE*, 1998, vol. 31, no. 3.
[50] Shirwani R, Gulzar S, Asim M, Umair M, Al-Rashid MA. Control of vehicular emission using innovative energy solutions comprising of hydrogen for transportation sector in Pakistan: A case study of Lahore City. Int J Hydrogen Energy 2020;45(32):16287–97.
[51] Plass Jr H, Barbir F, Miller H, Veziroğlu T. Economics of hydrogen as a fuel for surface transportation. Int J Hydrogen Energy 1990;15(9):663–8.
[52] Kale K, Dahake M. The effect of HHO and biodiesel blends on performance and emission of diesel engine-A review. Int J Curr Eng Technol 2016;5:1–9.
[53] Mathai R, Malhotra R, Subramanian K, Das L. Comparative evaluation of performance, emission, lubricant and deposit characteristics of spark ignition engine fueled with CNG and 18% hydrogen-CNG. Int J Hydrogen Energy 2012;37(8):6893–900.
[54] Çakmak A, Girisen AR, Ozcan H. Effects of hydroxy gas addition on the performance and emission characteristics of liquefied petroleum gas-powered lean-operated spark-ignition engine. SAE Int J Fuels Lubr 2021;14(1):41–54.
[55] Falahat A, Hamdan M, Yamin J. Engine performance powered by a mixture of hydrogen and oxygen fuel obtained from water electrolysis. Int J Automot Technol 2014;15:97–101.
[56] Hashem GT, Al-Dawody MF, Sarris IE. The characteristics of gasoline engines with the use of LPG: An experimental and numerical study. Int J Thermofluids 2023;18:100316.
[57] Ishola NB, Epelle EI, Betiku E. Machine learning approaches to modeling and optimization of biodiesel production systems: State of art and future outlook. Energ Conver Manage 2024;X:100669.
[58] Mangesha YK, Nallamothu RB, Ancha VR, Tefera NT. Optimization, Production, and characterization of cottonseed methyl ester based on Box-Behnken in response surface design and gas Chromatography-Mass spectrum analysis. Energy Convers Manage: X 2024;23:100619.
[59] Yameen MZ, et al. Biodiesel production from marine macroalgae Ulva lactuca lipids using novel Cu-BTC@ AC catalyst: Parametric analysis and optimization. Energy Convers Manage: X 2024;23:100628.
[60] S. M. W. ul Hasnain, A. S. Farooqi, O. Singh, N. H. Ayuni, B. V. Ayodele, and B. Abdullah, "Response surface optimization of hydrogen-rich syngas production by the catalytic valorization of greenhouse gases (CH4 and CO2) over Sr-promoted Ni/SBA-15 catalyst," *Energy Conversion and Management: X,* vol. 20, p. 100451, 2023.
[61] Caligiuri C, Renzi M, Antolini D, Patuzzi F, Baratieri M. Optimizing the use of forestry biomass producer gas in dual fuel engines: A novel emissions reduction strategy for a micro-CHP system. Energy Convers Manage: X 2023;20:100498.
[62] Khumthai W, Dujjanutat P, Muanruksa P, Winterburn J, Kaewkannetra P. Process optimization for the valorization of plastic waste into fuel additive production under the zero waste concept. Energy Convers Manage: X 2022;15:100231.
[63] Tefera NT, Nallamothu RB, Alemayehu G, Kefale Y. Optimization, characterization, and GC-MS analysis of CSOME produced using alkali catalyzed transesterification. Energy Convers Manage: X 2024;22:100549.
[64] Doppalapudi AT, Azad AK, Khan M, Oo AMT. Optimization and simulation of Tucuma and Ungurahui biodiesel process parameters and their effects on fuel properties. Energy Convers Manage: X 2024;24:100721.
[65] Ahmad M, et al. Sustainable and eco-friendly synthesis of biodiesel from novel and non-edible seed oil of Monotheca buxifolia using green nano-catalyst of calcium oxide. Energy Convers Manage: X 2022;13:100142.
[66] Chang M-H, Chen W-H, Wu D-R, Ghorbani M, Rajendran S, Daud WMAW. Analysis of vacuum operation on hydrogen separation from H2/H2O mixture via Pd membrane using Taguchi method, response surface methodology, and multivariate adaptive regression splines. Energ Conver Manage 2024;X:100645.
[67] Ghanbari M, Mozafari-Vanani L, Dehghani-Soufi M, Jahanbakhshi A. Effect of alumina nanoparticles as additive with diesel–biodiesel blends on performance and emission characteristic of a six-cylinder diesel engine using response surface methodology (RSM). Energy Convers Manage: X 2021;11:100091.
[68] Taghinezhad J, Alimardani R, Masdari M, Mahmoodi E. Performance optimization of a dual-rotor ducted wind turbine by using response surface method. Energy Convers Manage: X 2021;12:100120.
[69] Paneerselvam P, Panithasan MS, Venkadesan G. RSM optimization of ultrasound-assisted melia dubia oil extraction with green solvents and their suitability for diesel engine applications. Renew Energy 2024;222:119925.
[70] El-Kassaby MM, Eldrainy YA, Khidr ME, Khidr KI. Effect of hydroxy (HHO) gas addition on gasoline engine performance and emissions. Alex Eng J 2016;55(1):243–51.
[71] Babu J, et al. Production of HHO gas in the water-electrolysis unit and the influences of its introduction to CI engine along with diesel-biodiesel blends at varying injection pressures. Int J Hydrogen Energy 2024;52:865–85.
[72] J. P. Holman, "Experimental methods for engineers eighth edition," 2021.
[73] Y. Doğu, A. A. Yontar, and E. Kantaroğlu, "Experimental investigation of effects of single and mixed alternative fuels (gasoline, CNG, LPG, acetone, naphthalene, and boron derivatives) on a commercial i-DSI engine," *Energy Sources, Part A: Recovery, Utilization, and Environmental Effects,* pp. 1-20, 2020.
[74] Ma F, Wang Y, Liu H, Li Y, Wang J, Zhao S. Experimental study on thermal efficiency and emission characteristics of a lean burn hydrogen enriched natural gas engine. Int J Hydrogen Energy 2007;32(18):5067–75.
[75] A. Jones and R. Evans, "Comparison of burning rates in a natural-gas-fueled spark ignition engine," 1985.
[76] A. A. Yontar and Y. Doğu, "Experimental and numerical investigation of effects of CNG and gasoline fuels on engine performance and emissions in a dual sequential spark ignition engine," *Energy Sources, Part A: Recovery, Utilization, and Environmental Effects,* vol. 40, no. 18, pp. 2176-2192, 2018.
[77] Ristovski Z, Jayaratne E, Morawska L, Ayoko G, Lim M. Particle and carbon dioxide emissions from passenger vehicles operating on unleaded petrol and LPG fuel. Sci Total Environ 2005;345(1–3):93–8.
[78] Jahirul MI, Masjuki HH, Saidur R, Kalam M, Jayed M, Wazed M. Comparative engine performance and emission analysis of CNG and gasoline in a retrofitted car engine. Appl Therm Eng 2010;30(14–15):2219–26.
[79] Gad M, et al. Impact of oxy-hydrogen enriched gasoline on petrol engine performance and emissions. J Therm Anal Calorim 2022;147(23):13793–803.
[80] Aydin K, Kenanoğlu R. Effects of hydrogenation of fossil fuels with hydrogen and hydroxy gas on performance and emissions of internal combustion engines. Int J Hydrogen Energy 2018;43(30):14047–58.
[81] Darade P, Dalu R. Investigation of performance and emissions of CNG fuelled VCR engine. Emerg Technol Adv Eng 2013;3(1):77–83.
[82] Al-Hasan M. Effect of ethanol–unleaded gasoline blends on engine performance and exhaust emission. Energ Conver Manage 2003;44(9):1547–61.
[83] Ma F, et al. Performance and emission characteristics of a spark-ignition (SI) hydrogen-enriched compressed natural gas (HCNG) engine under various operating conditions including idle conditions. Energy Fuel 2009;23(6):3113–8.
[84] Arat HT, Baltacioglu MK, Özcanli M, Aydin K. Effect of using Hydroxy–CNG fuel mixtures in a non-modified diesel engine by substitution of diesel fuel. Int J Hydrogen Energy 2016;41(19):8354–63.
[85] Arjun T, Atul K, Muraleedharan AP, Walton PA, Bijinraj P, Raj AA. A review on analysis of HHO gas in IC engines. Mater Today Proc 2019;11:1117–29.
[86] Farooq MS, Ali U, Farid MM, Mukhtar T. Experimental investigation of performance and emissions of spark ignition engine fueled with blends of HHO gas with gasoline and CNG. Int J Therm Environ Eng 2021;18:27–34.
[87] Tabar AR, Hamidi AA, Ghadamian H. Experimental investigation of CNG and gasoline fuels combination on a 1.7 L bi-fuel turbocharged engine. Int J Energy Environ Eng 2017;8:37–45.
[88] P. Bielaczyc, A. Szczotka, and J. Woodburn, "A comparison of exhaust emissions from vehicles fuelled with petrol, LPG and CNG," in *IOP Conference Series: Materials Science and Engineering*, 2016, vol. 148, no. 1: IOP Publishing, p. 012060.
[89] A. M. De Morais, M. A. M. Justino, O. S. Valente, S. de Morais Hanriot, and J. R. Sodré, "Hydrogen impacts on performance and CO2 emissions from a diesel power generator," *international journal of hydrogen energy,* vol. 38, no. 16, pp. 6857-6864, 2013.

[90] Usman M, Saleem MW, Saqib S, Umer J, Naveed A, Hassan ZU. SI engine performance, lubricant oil deterioration, and emission: A comparison of liquid and gaseous fuel. Adv Mech Eng 2020;12(6):1687814020930451.
[91] Hu E, Huang Z, Liu B, Zheng J, Gu X, Huang B. Experimental investigation on performance and emissions of a spark-ignition engine fuelled with natural gas–hydrogen blends combined with EGR. Int J Hydrogen Energy 2009;34(1):528–39.
[92] Jafarmadar S, Majidi P. Experimental investigation of fuel effects (HHO_CNG) on gasoline-based engine performance. Fuel Combust 2020;13(3):121–35.
[93] P. Selvi Rajaram, A. Kandasamy, and P. Arokiasamy Remigious, "EFFECTIVENESS OF OXYGEN ENRICHED HYDROGEN-HHO GAS ADDITION ON DIRECT INJECTION DIESEL ENGINE PERFORMANCE, EMISSION AND COMBUSTION CHARACTERISTICS," *Thermal Science,* vol. 18, no. 1, 2014.
[94] Sherman G, Singh AP. Fuel efficiency and emissions reduction of hydroxy added gasoline fuel using HydroBoost technology. Int J Hydrogen Energy 2023;48(38):14511–26.